Remote Sensing of Environment 152 (2014) 441–466

Contents lists available at ScienceDirect

Remote Sensing of Environment

journal homepage: www.elsevier.com/locate/rse

Simulating SAR geometric distortions and predicting Persistent Scatterer densities for ERS-1/2 and ENVISAT C-band SAR and InSAR applications: Nationwide feasibility assessment to monitor the landmass of Great Britain with SAR imagery

Francesca Cigna *, Luke B. Bateson, Colm J. Jordan, Claire Dashwood

British Geological Survey, Natural Environment Research Council, Nicker Hill, Keyworth, NG12 5GG, United Kingdom

ARTICLE INFO

Article history:
Received 13 March 2014
Received in revised form 24 June 2014
Accepted 28 June 2014
Available online xxxx

Keywords:
Synthetic Aperture Radar
Feasibility
Layover
Shadow
Persistent Scatterers
PS density
InSAR
Radar Interferometry
Land surface processes

ABSTRACT

We assess the feasibility of monitoring the landmass of Great Britain with satellite Synthetic Aperture Radar (SAR) imagery, by analysing ERS-1/2 SAR and ENVISAT IS2 Advanced SAR (ASAR) archive data availability, geometric distortions and land cover control on the success of (non-)interferometric analyses. Our assessment both addresses the scientific and operational question of whether a nationwide SAR-based monitoring of ground motion would succeed in Great Britain, and helps to understand controlling factors and possible solutions to overcome the limitations of undertaking SAR-based imaging of the landmass. This is the first time such a nationwide assessment is performed in preparation for acquisition and processing of SAR data in the United Kingdom, and any other country in the world. Analysis of the ERS-1/2 and ENVISAT archives reveals potential for multi-interferogram SAR Interferometry (InSAR) for the entirety of Britain using ERS-1/2 in descending mode, with 100% standard image frames showing at least 20 archive scenes available. ERS-1/2 ascending and both ENVISAT modes show potential for non-interferometric and single-pair InSAR for the vast majority of Britain, and multi-interferogram only for 13% to 38% of the available standard frames. Based on NEXTMap® Britain Digital Terrain Model (DTM) we simulate SAR layover, foreshortening and shadow to the ERS-1/2 and ENVISAT Lines-Of-Sight (LOS), and quantify changes of SAR distortions with variations in mode, LOS incidence angles and ground track angles, local terrain orientation, and the effect of scale due to the input DTM resolution. The simulation is extended to the ~230,000 km^2 landmass, and shows limited control of local topography on the radar terrain visibility. According to the 50 m to 5 m DTM-based simulations, ~1.0–1.4% of Great Britain could potentially be affected by shadow and layover in each mode. Only ~0.02–0.04% overlapping between ascending and descending mode distortions is found, this indicating the negligible proportion of the landmass that cannot be monitored using either imaging mode. We calibrate the CORINE Land Cover 2006 (CLC2006) using Persistent Scatterer (PS) datasets available for London, Stoke-On-Trent, Newcastle and Bristol, to quantify land cover control on the PS distribution and characterise the CLC2006 classes in terms of the potential PS density they could provide. Despite predominance of rural land cover types, we predict potential for over 12.8 M monitoring targets for each acquisition mode using a set of image frames covering the entire landmass. We validate our assessment by processing with the Interferometric Point Target Analysis (IPTA) 55 ERS-1/2 SAR scenes depicting South Wales between 1992 and 1999. Although absolute differences between predicted and observed target density are revealed, relative densities and rankings among the various CLC2006 classes are found constant across the calibration and validation datasets. Rescaled predictions for Britain show potential for a total of 2.5 M monitoring targets across the landmass. We examine the use of the topographic and land cover feasibility maps for landslide studies in relation to the British Geological Survey's National Landslide Database and DiGMapGB mass movement layer. Building upon recent literature, we finally discuss future perspectives relating to the replication of our feasibility assessment to account for higher resolution SAR imagery, new Earth explorers (e.g., Sentinel-1) and improved processing techniques, showing potential to generate invaluable sources of information on land motions and geohazards in Great Britain.

* Corresponding author.
E-mail address: fcigna@bgs.ac.uk (F. Cigna).

http://dx.doi.org/10.1016/j.rse.2014.06.025
0034-4257/

1. Introduction

The possibility of mapping historical and recent land motions over wide areas of the Earth's surface with satellite differential Synthetic Aperture Radar Interferometry (InSAR) (e.g., Rosen et al., 2000) is increasingly stimulating interest within the geohazard community, especially with respect to operational monitoring of hazards threatening population and infrastructure, both in and outside Europe (Bally, 2012). InSAR-derived ground motion maps covering regions extending several thousands of square kilometres have been generated using C-band SAR images acquired between 1992 and 2010 by the European Space Agency (ESA)'s ERS-1/2 and ENVISAT missions, and extensively exploited for geological hazard mapping purposes over the last years (e.g., ESA, 2009).

Full national InSAR coverage has already been achieved for Italy and The Netherlands with Persistent Scatterer Interferometry (PSI), with the aim of addressing a number of natural and anthropogenic hazards, and improving the understanding of land processes and dynamics. The Extraordinary Plan for Environmental Remote Sensing (EPRS-E) was the first project to monitor, countrywide, land motions with PSI technologies (Costabile, 2012). For the Italian territory (~300,000 km^2), the EPRS-E produced a database of millions of radar targets and their motion histories, which were generated by processing ~15,000 ERS-1/2 and ENVISAT archive images acquired between 1992 and 2010, and now being further extended with data from the COSMO-SkyMed constellation. More recently, an ~70,000 km^2 map depicting 1992–2010 terrain motions of the whole of the Netherlands and part of Germany and Belgium was produced by Delft University of Technology based on integration of levelling and GPS data with ~600 ERS-1/2 and ENVISAT scenes processed with PSI (Caro Cuenca, Hanssen, Hooper, & Arıkan, 2011). Land motions due to groundwater exploitation, tectonic motions and other geological and anthropogenic processes over half of the Greek mainland, northern Germany, the Scheldt estuary in The Netherlands, and western Turkey have also been mapped recently by the German Aerospace Center (DLR) with the ESA Terrafirma Wide Area Product (WAP) and based on 22 ERS-1/2 image frames, for an ~220,000 km^2 area (Adam, Rodriguez Gonzalez, Parizzi, & Liebhart, 2011). This product was developed and validated in view of upcoming InSAR services based on Sentinel-1 Terrain Observation by Progressive Scans SAR (TOPSAR) data.

All these nationwide examples prove the importance of these processing techniques and their scientific impact, as well as the interest – especially in Europe – of various end-users in such types of products, which include but are not limited to, geological surveys, civil protection authorities and land use planners.

Building upon these successful achievements, our research aims to evaluate and map the potential of interferometric (e.g., InSAR, PSI, SBAS or Small Baseline Subset) and non-interferometric (e.g., amplitude change detection) techniques to monitor ground motion, geohazards and land changes in Great Britain. The entire chain comprising the acquisition of SAR imagery, its processing with (non-)InSAR techniques, analysis, modelling and interpretation requires significant resources in terms of data costs (if not under research, free licensing agreements), software (especially if commercial), man-power, computing facilities, and data storage space. To optimise the use of these resources, it is fundamental to assess a priori the suitability of SAR data and their processing techniques to image the territory of interest.

Past InSAR applications in and outside Europe have shown that the quality and quantity of ground motion information are controlled not only by the availability of image stacks over the areas to monitor (e.g., Crosetto, Monserrat, Iglesias, & Crippa, 2010), but also by local topographic setting and land use (e.g., Nico, Oliveira, Catalão, & Zêzere, 2009; Notti, Meisina, Zucca, & Colombo, 2011; Plank, Singer, Minet, & Thuro, 2012; Riddick, Schmidt, & Deligne, 2012). Indeed, the visibility of the target areas to various satellite sensors depends on the combination of local slope orientation with the acquisition geometry and mode of the satellite sensor Line-Of-Sight (LOS). Non-ideal geometrical configurations may result in image distortions (e.g., Gelautz, Frick, Raggam, Burgstaller, & Leberl, 1998), induce significant underestimation of land motions, or even hamper the identification of reflective targets over the observed areas (e.g., Barboux, Delaloye, Strozzi, Collet, & Raetzo, 2011; Cigna, Bianchini, & Casagli, 2013; Herrera et al., 2013). Moreover, the spatial coverage of InSAR products is controlled by land cover, and achieving InSAR results in rural and mountainous environments can be challenging, due to SAR phase decorrelation occurring as an effect of temporally variable, observed surfaces (e.g., Ferretti, Prati, & Rocca, 2001; Sowter, Bateson, Strange, Ambrose, & Syafiudin, 2013; Strozzi, Ambrosi, & Raetzo, 2013). The a priori determination of where good scatterers will be identified is an important question to answer before undertaking InSAR monitoring of an area of interest (Plank, Singer, & Thuro, 2013).

To assess the feasibility of non-interferometric, InSAR and PSI techniques to monitor the landmass of Great Britain, we analyse the ERS-1/2 and ENVISAT SAR archive image availability, and analyze the interactions of topographic and land cover constraints for SAR-based applications. Our assessment combines the simulation of the effects of topography on the visibility of target areas to the satellite SAR acquisition geometry, with the quantification of land cover control on the success of PSI processing of archive SAR data via prediction of radar target densities. These effects are summarized into a series of feasibility maps, which help to understand where SAR-based applications are likely to succeed and where not. These maps are examined in relation to geohazard layers produced by the British Geological Survey (BGS), and validated by processing a long stack of ERS-1/2 SAR scenes acquired over South Wales. The future perspectives relating to the implementation of these maps are discussed with respect to higher spatial and temporal resolution SAR imagery, such as the existing TerraSAR-X and COSMO-SkyMed constellations operating in X-band, and the C-band Sentinel-1 mission, with the first satellite, Sentinel-1A, launched on 3rd April 2014 (ESA, 2014a, 2014b). We also discuss the potential of improved processing techniques which can provide denser and often more complete spatial coverage of SAR-derived results even in rural areas, where achieving C- or X-band InSAR results can be challenging.

This feasibility study both addresses the scientific and operational question of whether nationwide SAR-based monitoring of ground motion would succeed in Great Britain, and helps to understand controlling factors and possible solutions to overcome the limitations of undertaking such monitoring. This is the first time such a nationwide assessment is performed in the United Kingdom and, to the best of our knowledge, in any other country in the world. Methods developed by other authors are adapted and combined here to overcome and compensate for their limitations and achieve unprecedented accuracies in the simulation of SAR image distortions. Analysis of the feasibility is specifically focussed on ERS-1/2 and ENVISAT data archives, to assess how these would perform to create a baseline nationwide InSAR dataset as a background land motion product in view of higher spatial and temporal resolution SAR sensors onboard forthcoming and existing Earth explorers.

2. Nationwide feasibility assessment in Great Britain

The target of our study is Great Britain, comprising an area of ~230,000 km^2 made up of a main landmass and minor islands and islets. Its land cover varies from densely urbanised cities like London, to non-irrigated arable land and pastures which dominate England and part of Wales. Scotland, the mountainous regions of Wales, the North York Moors and the Pennines in central-northern England comprise natural grassland, woodland, peat bog, sparsely vegetated areas, heathland and moors (Fig. 1a). Most of the landmass is dominated by gentle topography and steepness of slopes in the hilly and mountain regions generally does not exceed ~15–20° (Fig. 1b). Statistics for NEXTMap® Digital Terrain Model (DTM) at 50 m resolution show that average slopes (β) are ~5°, and that the majority of Great Britain (~95%) is characterised

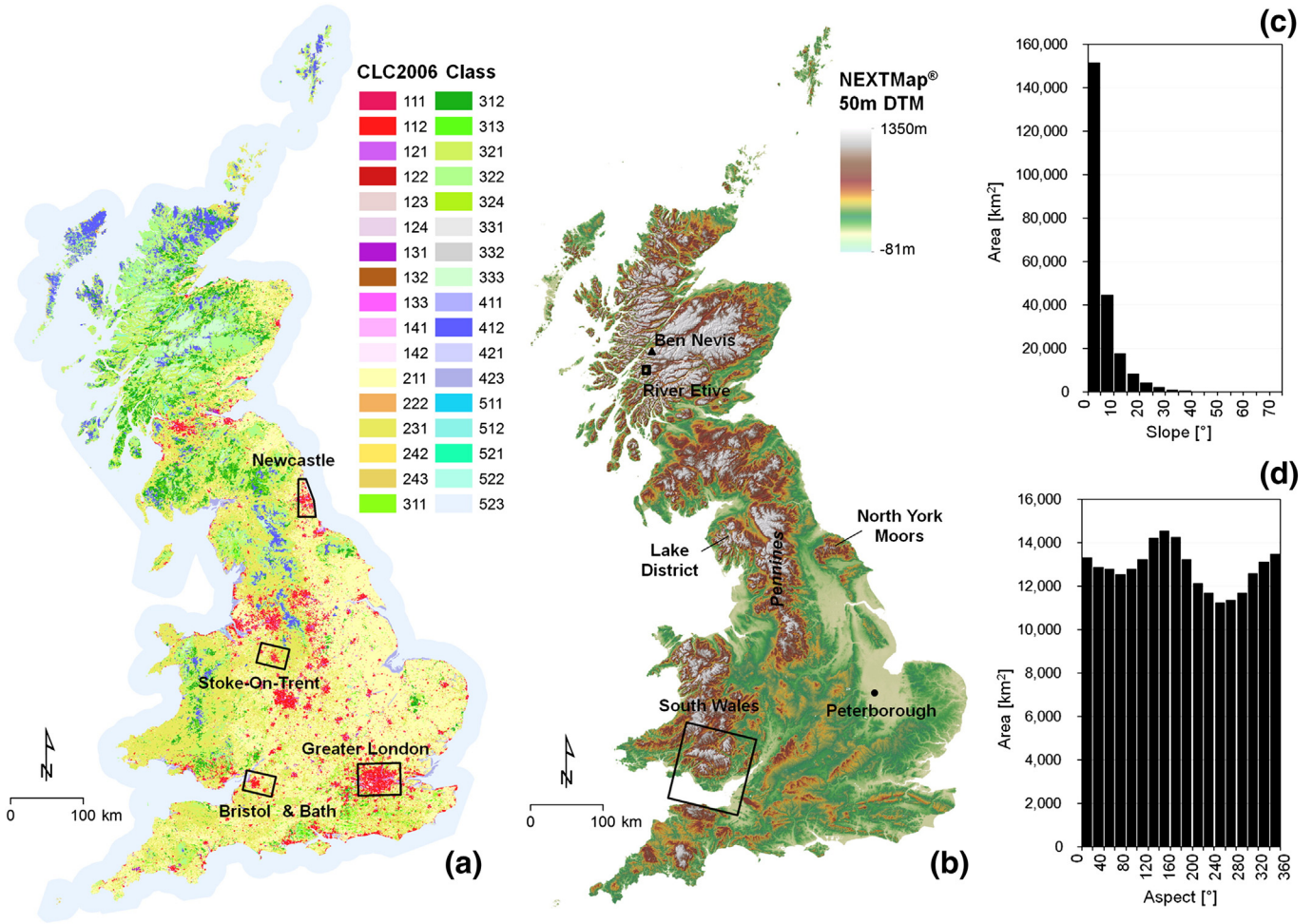

Fig. 1. (a) Land cover of Great Britain from the CORINE Land Cover map 2006 (CLC2006). CLC2006 classes associated with legend codes are summarized in Table 2. (b) Topography and distribution of (c) terrain slopes and (d) aspects of Great Britain from NEXTMap® DTM at 50 m resolution. Location of PS datasets used for calibration is overlapped onto (a), whilst the sites used for validation of the simulated geometric distortions and calibrated CLC2006, i.e. the River Etive in Scotland, and South Wales, are shown in (b). British National Grid; Projection: Transverse Mercator; Datum: OSGB 1936. Vertical Datum: OSGM91. NEXTMap® Britain © 2003, Intermap Technologies Inc., All rights reserved. CLC2006 © 2007, European Environment Agency (EEA).

by $\beta < 20°$. Only ~5% of the territory shows steeper values (Fig. 1c). The latter are observed, for instance, in Scotland, the Lake District and Wales, at the highest elevations (e.g., over +1340mOD at Ben Nevis in the Highlands, Scotland). Maximum β of ~75° is observed only at very few locations, e.g. along some coastal areas in Scotland. Most of the landmass (~95%) has heights lower than +535mOD, and the lowest elevations are mainly found in Norfolk and around Peterborough, and the Cambridgeshire (Fig. 1b).

Geohazards affecting Great Britain include natural compaction of recent river deposits, shrink-swell clays, shallow and deep-seated landsliding, land subsidence/uplift due to groundwater abstraction/recharge, and ground motions induced by human activities such as engineering works, underground constructions, new housing and industrial developments, and excavations and mine-water management in active and abandoned mining areas (e.g., Farrant & Cooper, 2008; Gibson, Culshaw, Dashwood, & Pennington, 2013; Jones & Jefferson, 2012). Monitoring and understanding a multi-hazard environment have long been a challenging task primarily due to overlapping of hazard type and interaction of natural and anthropogenic processes, different spatial and temporal scales, and the variety of motion types and respective kinematics affecting this region.

Imaging Great Britain from satellite platforms is influenced by its weather. Long-term averages for the latest 30-year long period (i.e. 1981–2010) show that more than 90% of the landmass has yearly records of over 100 days with more than 1 mm precipitation, over 600 mm rainfall, and less than ~1500 h sunshine duration on average (Met Office, 2013a, 2013b). In light of the temperate maritime and varied climate of the island and the UKCIP02 (UK Climate Impacts Programme 2002) climate change scenarios for the UK (Hulme et al., 2002) which highlights an increase in the frequency of heavy winter precipitation and consequent changes in evapo-transpiration rates across the landmass, active remote sensing technologies (e.g., radar sensors) are particularly effective to monitor the landmass. This is due to the capabilities of microwaves to penetrate clouds and image the surface independently of weather conditions and cloud coverage, as opposed to the difficulties of optical sensors to operate in such conditions.

In this regard, an increasing interest in monitoring geohazards affecting Great Britain with satellite InSAR has developed over the last decade. Since 2003, via the projects ESA Terrafirma in 2003–2013, Land Levels funded by the Department for Environment, Food and Rural Affairs (DEFRA) and the Environment Agency (EA) in 2003–2006, and EC-FP7 PanGeo in 2011–2014, a number of ground motion services employing InSAR have been delivered to and by the BGS, as well as to national and local authorities (e.g., ESA, 2009). By exploiting ERS-1/2 and ENVISAT archives, these studies provided new insights into ground and building motion histories for a number of areas of the UK, including Stoke-on-Trent, Bristol and Bath, London and the Northumberland region (e.g., Aldiss et al., 2014; Banton et al., 2013; Culshaw, Tragheim, Bateson, & Donnelly, 2006). Other individual studies have also been carried out more recently, such as a

validated ENVISAT PSI analysis in the city of Nottingham (Leighton, Sowter, Tragheim, Bingley, & Teferle, 2013), and Intermittent SBAS (ISBAS) studies of South Derbyshire and Leicestershire (Sowter et al., 2013), and South Wales coalfields (Bateson, Cigna, Boon, & Sowter, in press). These reveal the remarkable potential of InSAR to understand a variety of surface processes, including both natural and anthropogenic geohazards operating in Great Britain. The question has always remained however, whether national ground monitoring from InSAR is feasible in Britain.

To assess how SAR-based analyses such as single-pair and multi-interferogram differential InSAR (e.g., PSI and SBAS) and non-interferometric techniques would perform across Great Britain, we employ a four-phase methodology, schematically represented in the flow chart of Fig. 2 and summarized as follows:

Phase (1): Analysis of ESA's ERS-1/2 SAR and ENVISAT Advanced SAR (ASAR) archives to determine the number, distribution and temporal coverage of the available SAR scenes for the British landmass (see Section 2.1);

Phase (2): NEXTMap® Britain DTM-based simulation of SAR distortions based on orientation parameters of ERS-1/2 SAR and ENVISAT ASAR satellite LOS in ascending and descending modes, as described in Section 2.2;

Phase (3): CORINE Land Cover map 2006 (CLC2006) characterisation and calibration using external PS datasets already processed over various sites in Great Britain (see Section 2.3); and

Phase (4): Generation of geocoded ERS-1/2 scenes and identification of Point Target Candidates (PTC) for validation of simulated geometric distortion and calibrated land cover maps (see Section 3).

The methodology is developed and used for Great Britain, but can be exported to any other territory, provided the availability of relevant input data. In this respect, ERS-1/2 and ENVISAT archives, CLC2006 and NEXTMap® Britain can be replaced with other SAR archives, land cover maps and DTMs respectively, depending on availability for the analysed areas.

The usefulness of the feasibility maps generated for landslide research in Great Britain is discussed in Section 4 in relation to available landslide maps and databases. Further discussion is conducted in Section 5 on future perspectives of this assessment with higher resolution satellite data and newly developed processing approaches.

2.1. ERS-1/2 and ENVISAT C-band archive data availability

The generation of a complete picture of ground motion over target areas requires the availability of sufficiently long and populated stacks of SAR imagery. Higher accuracy of ground motion estimates, atmospheric phase components and height errors is achieved with greater numbers of images when processing a stack with multi-interferogram methods such as PSI and SBAS (e.g., Berardino, Fornaro, Lanari, & Sansosti, 2002; Ferretti et al., 2001). Usually, to undertake a multi-interferogram InSAR analysis at least ~15–20 images that were acquired using the same acquisition geometry (e.g., same mode, orbit and track) are required (e.g., Crosetto et al., 2010).

ESA's C-band image archives provide the most complete database of radar data for Great Britain, since they offer consistent and rich stacks of historical ERS-1/2 and ENVISAT data acquired for the entire landmass over the last two decades. In particular, there are more than 10,500 ERS-1/2 SAR images acquired between 1991 and 2001 (before failure of one gyroscope), and more than 3400 ENVISAT ASAR Image Swath 2 (IS2) mode images acquired between 2002 and 2010 (before the orbit lowering manoeuvre, and the extension orbit). These figures are based on available ascending and descending modes 100 by 100 km standard frames from ESA's client for Earth Observation (EO) Catalogue and

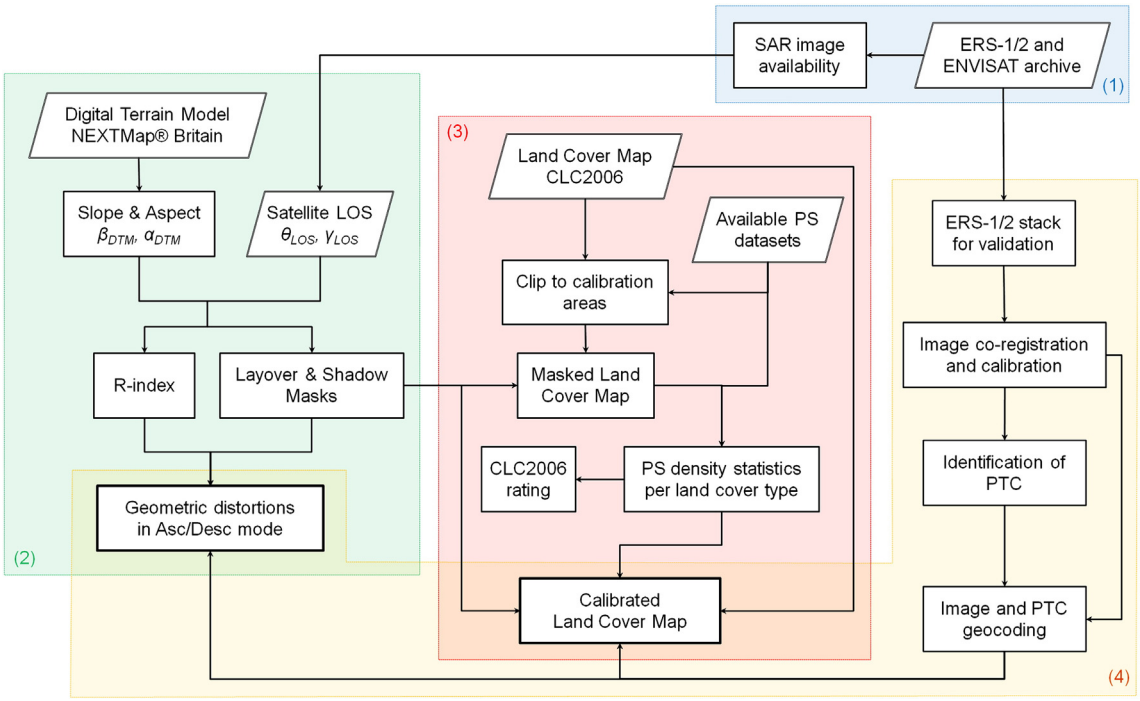

Fig. 2. Methodology for assessing the feasibility of InSAR and PSI techniques: Phase (1) ERS-1/2 and ENVISAT SAR archive analysis; Phase (2) geometric distortion simulation in ascending and descending modes; Phase (3) land cover map characterisation and calibration; Phase (4) generation of geocoded ERS-1/2 scenes and Point Target Candidates (PTC) for validation of SAR distortion and calibrated land cover maps. This methodology was developed and used for Great Britain, but can be exported to any other territory, provided relevant input data are available. In this flow chart, ERS-1/2 and ENVISAT archives, CLC2006 and NEXTMap® Britain can be replaced with other SAR archives, land cover maps and DTMs respectively, depending on availability.

Ordering Services, i.e. EOLI-SA multi-platform interactive tool. Evidently, many more scenes are available from the ERS-2 mission after early 2001 and from ENVISAT after 2010, but they are usually not combined with pre-2001 and post-2010 data due to differences in the Doppler centroid and satellite orbit characteristics respectively, and thus are not taken into account for the purposes of this analysis.

The availability of SAR C-band raw input data confirms the potential to perform single- and multi-interferogram ground motion analysis of geohazards, as well as non-interferometric studies. Fig. 3 shows the spatial distribution of the available ERS and ENVISAT data for the main, standard frames available over Great Britain, and provides average figures of:

- 65 ERS-1/2 SAR and 18 ENVISAT ASAR IS2 images for each image frame acquired along descending satellite orbits; and
- 20 ERS-1/2 and 13 ENVISAT IS2 images for each image frame acquired along ascending satellite orbits.

For the vast majority of Great Britain, all image stacks in either mode (ascending or descending) of both ERS-1/2 and ENVISAT provide sufficient data for non-interferometric and single-pair InSAR analysis. On the other hand, availability of image stacks composed of at least 20 scenes is revealed for 100% of the ERS-1/2 image stacks in descending mode, thus suggesting that the feasibility of multi-interferogram InSAR analyses with PSI or SBAS approaches can be guaranteed for the entirety of the landmass using these satellite stacks (Fig. 3b). Over 38% of the ERS-1/2 image stacks in ascending mode, and 37% and 13% for ENVISAT IS2 ASAR image stacks in descending and ascending modes respectively are composed of a sufficiently consistent number of scenes to perform multi-interferogram InSAR. This suggests that ERS ascending mode stacks, and both ENVISAT modes can cover with PSI or SBAS approaches substantial portions of the landmass but not its entirety.

These observations are clearly made with an understanding that further analysis of normal and temporal baselines of the available image stacks is necessary to verify whether interferometric phase correlation can be guaranteed across the available stacks (e.g., for SBAS applications with temporal baselines shorter than 4 years, and normal baselines smaller than 130–200 m; e.g., Berardino et al. (2002); Sowter et al. (2013)).

In addition to the availability of suitable SAR archives, the assessment of the feasibility of such historical analysis and any future monitoring with new Earth explorers (e.g., the Sentinel-1 constellation) requires appraisal of the topographic and land use constraints which impact on the distribution of image distortions, radar monitoring results and density of retrieved targets. Topographic and land cover effects

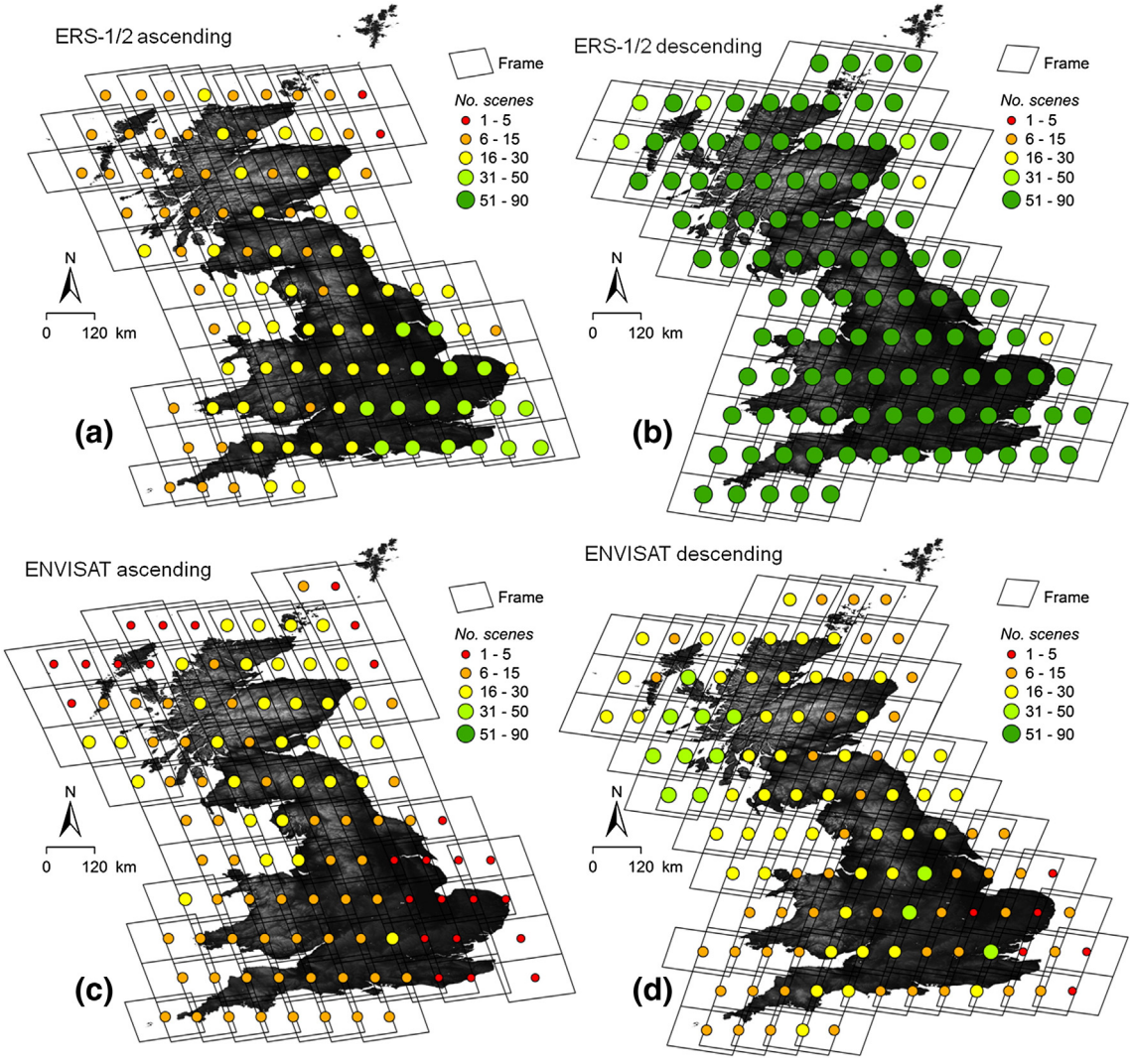

Fig. 3. Satellite SAR image availability over Great Britain: spatial distribution of the number of available scenes per ERS-1/2 (a–b) and ENVISAT (c–d) frames for the ascending and descending modes, overlapped onto shaded relief of NEXTMap® DTM at 50 m resolution. Datum: WGS84. NEXTMap® Britain © 2003, Intermap Technologies Inc., All rights reserved.

depend on the type and characteristics of input SAR data available to process indeed, and these are analysed and discussed in detail in the following Sections 2.2 and 2.3, with regard to ERS-1/2 and ENVISAT archive imagery.

2.2. Topographic visibility mapping and simulation of SAR distortions

Terrain visibility to the radar satellite sensor depends on the orientation of the employed satellite Line-Of-Sight (LOS) and radar acquisition geometry with respect to that of the surface. Visibility thereby varies within different portions of the same scene depending on local incidence angles which, in turn, are determined by local terrain slope and aspect. Depending on their effects, slant-range geometrical distortions can be classified in layover, foreshortening and shadow (e.g., Colesanti & Wasowski, 2006; Gelautz et al., 1998).

The presence of radar layover and shadow, either active or passive (e.g., Kropatsch & Strobl, 1990), prevents the application of both interferometric and non-interferometric techniques (e.g., Cigna, Bianchini, et al., 2013). Consequently the a priori identification of these distortions is essential to plan SAR-based analyses, especially over hilly and mountainous regions. On the other hand, assessment of the most suitable LOS geometry to ensure that the target area is visible to the employed sensor mode is strongly suggested prior to the acquisition of long SAR imagery stacks. The latter indeed might have significant costs, especially when employing high resolution sensors and requesting data acquisition for commercial applications.

Some approaches to model SAR distortions and terrain visibility were developed in the last two decades. Earlier examples are the simulation of layover and shadow regions based on DEMs and sensor acquisition parameters which are discussed by Kropatsch and Strobl (1990) and Gelautz et al. (1998). During the following decade, Colesanti and Wasowski (2006) analysed the visibility conditions of unstable slopes with different orientations and identified the ranges of aspect and slope which determine radar layover, foreshortening and shadow. Colombo et al. (2006) cross-combined the effects of topography and land use in Piedmont (Italy), and masked out layover and shadow regions by means of the approach of Kropatsch and Strobl (1990) using a 20 m resolution DTM. Cascini, Fornaro, and Peduto (2010) discussed and implemented the approach of a priori InSAR landslide visibility mapping in Campania (Italy), based on the assignment of simple conditions in terrain slope and aspects. Pourthie et al. (2010) developed the SARVisor tool to simulate layover and shadow areas to facilitate the selection of SAR acquisition modes for areas of interest. More recently, Notti, Davalillo, Herrera, and Mora (2010) and Notti et al. (2011) synthesized the effects of local topography into the R-index (i.e. Range-index) and tested it over the Tena Valley (Spain) and in Piedmont (Italy). Plank et al. (2012) also presented a GIS-based pre-survey InSAR procedure to predict areas of geometric distortions, which simulates layover and shadow by using DEMs and information on SAR acquisition mode. These latter authors observed, however, notable mismatch between simulated and processed distortions especially when DEMs at medium resolution are employed for either the simulation or the actual layover processing of the radar image used for validation.

In our research, we accounted for observations made by the above authors, and proved that our approach to simulate distortions based on DTMs overcomes limitations relating to single pixel-based assessments such as those by Cascini et al. (2010) and Notti et al. (2010), or procedures leading to notable discrepancies between modelled and processed image distortions.

2.2.1. DTM-based modelling of SAR distortions with layover and shadow masking and the R-index

To identify and model SAR geometrical distortions to the ascending and descending acquisition modes of the European satellites ERS-1/2 and ENVISAT in Great Britain, we combine and adapt the layover and shadow masking and R-index approaches respectively by Kropatsch and Strobl (1990) and Notti et al. (2010), and developed the methodology summarized in Fig. 2. This combined methodology not only compensates for the limitations touched on in the previous section, but also identifies univocally the three types of image distortions (i.e. foreshortening, layover and shadow) and their sub-types.

The topographic index R represents an indication of the ratio between the pixel size in slant and ground range geometry or 'pixel compression factor'. The severity of the pixel compression varies in relation to the local incidence angle (i.e., angle between the terrain surface normal and the radar beam), which in turn is determined by the LOS look or incidence angle (θ) and satellite ground track angle or heading angle (γ), and local terrain slope (β) and aspect (α) (see Fig. 4a). A simplified version of the formula proposed by Notti et al. (2011) to calculate R in the GIS environment follows:

$$R = \sin[\vartheta - \beta \cdot \sin(A)] \quad (1)$$

where A is the aspect correction factor, which is computed as $A = \alpha - \gamma$ for descending mode data, and $A = \alpha + \gamma + 180°$ for ascending mode data.

As discussed in Cigna, Bateson, Jordan, and Dashwood (2012) and hereafter, the sole use of R is not sufficient to identify all geometrical distortions. Indeed, although the R-index can successfully identify areas of good terrain visibility and foreshortening regions, it only accounts for the effects of 'active layover' (i.e. areas producing layover onto other ones) and can identify neither areas of 'passive layover' (i.e. regions over which active layover areas lay) nor shadows (either active or passive). To obtain a detailed understanding of the index, we studied Eq. (1) and the changes of R for the ascending and descending modes of ERS and ENVISAT data with 23° θ and ±14° γ, with varying terrain aspects (e.g., in Fig. 4b for the ascending mode). These values are those defining the average acquisition parameters for the British landmass (see also Section 2.2.2).

When the geometrical configuration of the slope and the LOS causes the slope to be in active layover (i.e., θ lower than β, for slopes facing the sensor), R takes on negative values between 0 and −1. Ascending and descending LOS produce distortions in slopes with opposing orientations, and east facing slopes have lower R in the descending mode rather than in the ascending, and west facing slopes vice versa (Fig. 4c–e). On the other hand, areas of foreshortening show R-index above 0 and up to $\sin(\theta)$. The latter represents the specific threshold to discriminate foreshortening from good visibility regions, and is here named R_0. Its value corresponds to that taken on by R for flat terrains, which is obtained by putting $\beta = 0$ in Eq. (1). Clearly, R_0 increases with increasing θ which in turn is controlled by the satellite LOS and acquisition modes. Using ERS and ENVISAT LOS configurations and assuming 23° θ and ±14° γ, R_0 equals +0.39 (Fig. 4b). Areas facing away from the sensor are characterised by sizes in ground range higher than in slant range but with favourable orientation (hence positive R), with values higher than R_0 and up to +1 (when the slope is parallel to the LOS).

Fig. 4c shows R-index changes due to β variations and reveals that, if $\beta < 67°$, R-index takes on its minimum value when the terrain is perpendicular to the LOS and layover effects are stronger, i.e. when A equals 90°. Flat slopes are all characterised by the same R-index value, irrespective of their α, whereas maximum R is taken on for slopes parallel to the LOS, i.e. when A equals 270°. By analysing Eq. (1) and Fig. 4c, it becomes apparent however that since both active shadow (in this case, occurring when $\beta > 67°$) and good visibility areas face away from the sensor, they are both characterised by high R-index and in particular, in the region between +0.92 and +1 for ERS and ENVISAT LOS. Indeed, when $\beta >$ 67° the R-index reaches +1, and the curves fold back to lower values as β increases and active shadow occurs. As a result, active shadow and good visibility cannot be discriminated by using the sole R-index, unless terrain orientation is further accounted for, e.g. by differentiating active shadow regions as those with $\beta > 67°$.

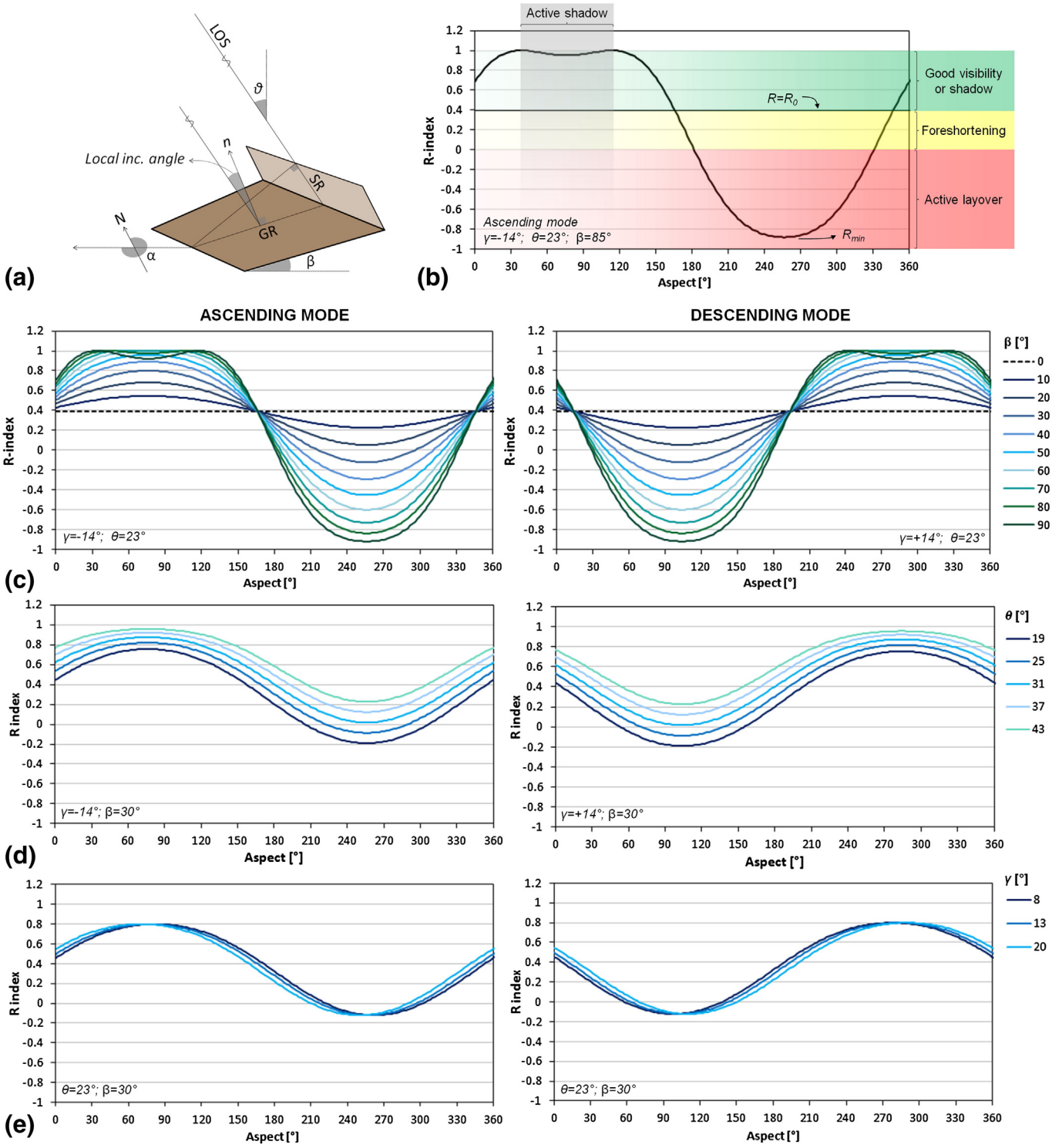

Fig. 4. Ground (GR) and slant (SR) range orientation of a DEM pixel (a) and R-index variations with LOS and local terrain orientation (b–e). (b) Example of identification of distortions in the R-index plot for the ascending mode of a right-looking SAR sensor with $\gamma = -14°$ and $\theta = 23°$, for a slope with $\beta = 85°$; and (c–e) changes in the R-index with (c) terrain slope β, (d) LOS incidence angle θ, and (e) satellite track angles γ, for the ascending and descending modes of ERS-1/2 and ENVISAT SAR imagery.

Neither 'passive layover' or 'passive shadow' can therefore be identified via sole use of the R-index, as only the local orientation of single pixels of a DEM is analyzed via R, and not their effects on and their interactions with surrounding areas. Analogous observations can be made for the visibility methods discussed by Colesanti and Wasowski (2006) and Cascini et al. (2010) who exploit single pixel-based approaches to determine the presence or absence of image distortions. The generation of shadow and layover masks by means of other approaches can complement this limitation. Kropatsch and Strobl (1990), for instance, map layover and shadow in the reference system of a DEM (e.g. geographic coordinates) by analysing local incidence angles and topographic profiles across-track, and can efficiently identify

the terrain visibility, both active and passive radar shadow, and both active and passive layover.

2.2.2. Simulated SAR distortions to ERS-1/2 and ENVISAT modes in Great Britain

To overcome the above limitations and optimise the DTM-based simulation, for our simulation in Great Britain the three geometric distortions and their sub-types were identified in the GIS environment as follows:

- *Foreshortening*: areas where $0 < R\text{-}index \leq R_0$, and not affected by either passive layover or passive shadow distortions based on the shadow and layover masking;
- *Layover*: using the layover masking, and then by identifying pixels where $-1 \leq R\text{-}index \leq 0$ (hence areas producing layover; 'active layover'), to discriminate 'active' from 'passive layover' regions; and
- *Shadow*: using the shadow masking, and then by discriminating areas where $R\text{-}index > R_0$ and slopes $> 90° - \theta$ (hence 'active shadow') from regions affected by passive distortions.

To define the orientation of the ascending and descending LOS of ERS-1/2 SAR and ENVISAT ASAR IS2 for the British landmass, we employed constant LOS θ of 23°, and γ of $\pm 14°$. Variations of θ across the swath (from the near to the far range of each image frame) and of γ across the landmass (from approximately 50° to 59°N latitudes) were not accounted for at this stage of the modelling. Hence constant values were assumed for all Great Britain, with an understanding that this generalization might result in inaccurate estimations at the margins of each image frame (i.e., in the far and near range), and for the northernmost and southernmost latitudes (i.e., highest and lowest satellite frame numbers). Implications of these assumptions are discussed further in Section 2.2.2. Layover and shadow masks were generated by modelling the satellite sensor location using hill-shading and shadowing models, with azimuth and altitude angles being defined accounting for the sensor LOS orientation parameters θ and γ.

As a first approximation-screening for our higher resolution studies, we performed an initial test based on the Shuttle Radar Topography Mission (SRTM) Digital Surface Model (DSM) V4 at 90 m resolution produced by NASA in 2000, which is briefly presented in Cigna et al. (2012). SRTM-based nationwide maps of R-index, shadow and layover for both orbital modes suggested that topography is not the major limitation for SAR-based studies over most of Great Britain, with layover affecting only 0.6% of the landmass (per mode) and no shadow identified (Table 1). The latter is due to the absence in the SRTM data of slopes steeper than 67°, rather than actual absence of this distortion type.

Local terrain orientation for Great Britain was assessed here in increased detail, by employing the 5 m airborne InSAR NEXTMap® Britain Digital Terrain Model (DTM) produced by Intermap Technologies in 2001–2003, and its 10 m and 50 m derivatives. This approach allowed us to analyse the topographic visibility of the territory by first starting at small scales (i.e. national and county scales) before going into detail at the local scale (i.e. single slopes), and to compensate for limitations relating to the use of low resolution topographic models. A further goal of our multi-scale and multi-resolution approach was to find the most suitable compromise between the various resolutions and their capabilities to depict topographic complexity, that was revealed during the validation in Wales (see Section 3) and our analysis of the effect of scale (see Section 2.2.3). DTMs rather than DSMs were used in order to filter out topographic components related to buildings, trees, and other surface features. The latter were removed from the original DSM data by Intermap prior to product delivery. Derived 10 m and 50 m resolution DTMs were generated subsequently, by resampling the original 5 m data with a cubic convolution algorithm. Clearly, the use of the DTM for our simulation was to the detriment of identifying image distortions produced by manmade structures. This approach, on the other hand, allowed avoidance of misleading effects which would have been caused by the presence of trees in the input data for the simulation of terrain visibility.

The general presence of gentle topography in Great Britain results in NEXTMap®-based R-index, shadow and layover masks generally revealing limited control of the terrain on its visibility to SAR sensors (Fig. 5). Exceptions are hilly regions, where visibility is controlled by the satellite acquisition mode (ascending or descending). For these areas, it is apparent that E-facing slopes are generally best depicted using ascending mode LOS, whilst W-facing slopes are better imaged using the descending geometry.

By employing the approach of Kropatsch and Strobl (1990), we determined total areas of shadow within Great Britain as small as 0.0325 km^2 in ascending, and 0.5425 km^2 in descending mode, as modelled using the NEXTMap® DTM at 50 m (Fig. 5a,d and Table 1). These figures clearly differ from the SRTM-based simulations for which no shadow was determined due to the absence of slopes steeper than 67°. Total areas of layover (including active and passive) are 2225 km^2 in ascending, and 2298 km^2 in descending mode (Fig. 5b,e). Of these, 1074 km^2 in ascending and 1088 km^2 in descending mode are active layover regions, which were determined as a subset of total layover, by considering DTM pixels showing R between −1 and 0. Total extension of layover and shadow distortions for the landmass is ~1.0% in each imaging mode (Table 1). The results of the layover and shadow maps show that, for almost the entire island, layover effects observed for the descending geometry over slopes facing E, can be avoided by employing the ascending one, and vice versa for W-facing slopes (Fig. 5c,f). Indeed, areas resulting in layover or shadow distortions in both geometries (i.e. areas that cannot be monitored using SAR imagery with either orbital mode) extend 48.8 km^2 according to the 50 m DTM-based simulation, covering 0.02% of Great Britain.

Areas of foreshortening were determined by considering R-index of 0 to +0.39, and resulted extended 106,621 km^2 (~46.1% of the landmass) in ascending, and 116,301 km^2 (~50.4%) in descending mode. The absence of any type of distortions is observed over around 122,245 km^2 (~52.9%) in ascending, and 112,001 km^2 (~48.6%) in descending mode (Fig. 5b,e). It is also apparent that, as an average over the entire territory, SAR distortions are slightly more extended in the descending mode rather than ascending. This might be a consequence of terrain orientations of Great Britain which show pronounced

Table 1
Total areas of simulated ERS-1/2 and ENVISAT SAR shadow and layover (including both active and passive distortions) across Great Britain, based on the 90 m resolution SRTM DSM, and the 50 m, 10 m and 5 m resolution NEXTMap® DTMs. Regions affected by shadow or layover distortions in both modes are also shown. Extensions are expressed in terms of both their total areas (in km^2) and percentages with respect to the entirety of the landmass.

		ERS-1/2 and ENVISAT ascending mode			ERS-1/2 and ENVISAT descending mode			Distortions in both modes	
Input data	Resolution [m]	Shadow [km^2]	Layover [km^2]	Total [%]	Shadow [km^2]	Layover [km^2]	Total [%]	[km^2]	[%]
SRTM DSM	90	0	1411	0.6%	0	1474	0.6%	18.0	0.01%
NEXTMap® DTM	50	0.0325	2225	1.0%	0.5425	2298	1.0%	48.8	0.02%
	10	0.3743	3034	1.3%	2.8215	2996	1.3%	78.2	0.03%
	5	0.8629	3228	1.4%	4.5893	3164	1.4%	87.5	0.04%

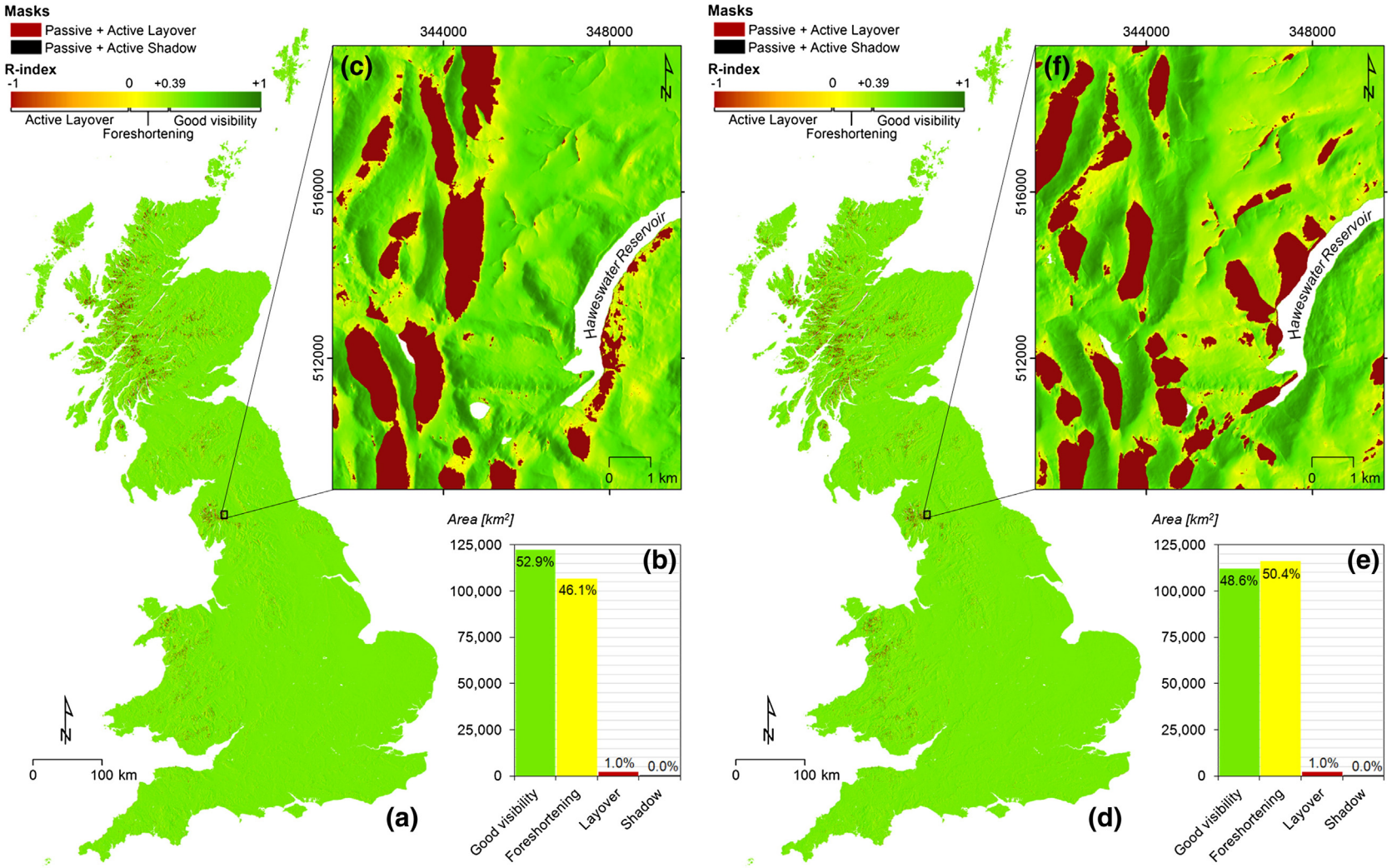

Fig. 5. Identification of image distortions to the ERS-1/2 and ENVISAT ascending (a–c) and descending (d–f) modes over Great Britain. Histograms (b) and (e) show total area statistics of (a) and (d) which are based on the 50 m NEXTMap® DTM. Zooms in (c) and (f) show the results based on the 10 m NEXTMap® DTM for the area of the Haweswater Reservoir in the Lake District, England, in the ascending and descending modes, respectively. British National Grid; Projection: Transverse Mercator; Datum: OSGB 1936.

predominance of south-east facing slopes, i.e. 135–180° α (Fig. 1d). These are best imaged by using the ascending geometry.

2.2.3. Effect of scale induced by the input DTM resolution

It is worth noting that the above statistics and extension of the areas affected by distortions are based on NEXTMap® DTM data with 50 m pixels. This implies that their estimates are performed in terms of multiples of the unit pixel area, i.e. 0.0025 km^2, and are also influenced by the lower level of topographic detail of medium resolution data. Similarly, 10 m DTM-based estimates are related to 0.0001 km^2 unit areas, 5 m ones to 0.000025 km^2 unit areas, and 90 m SRTM ones to 0.081 km^2 unit areas.

The use of higher resolution DTMs can of course increase the accuracy of modelled distortions, by improving the identification of their exact boundaries and extension, better depicting topographic features and complexity, steep and uneven terrains which are smoothed by lower resolution data.

Gelautz et al. (1998) already highlighted that the input DEM resolution has significant importance for SAR image simulation, and that simulated data should have comparable or greater pixel size with respect to that of the input DEM. Their observations suggest that simulation of distortions for ERS-1/2 and ENVISAT data should be based on input DTMs with pixel sizes lower than ~25–30 m. Moreover, the selection of the best resolution to map these distortions has to be determined by also accounting for the variations of the SAR pixel resolution in the ground range direction and across the scene due to the presence of topography and local variations of incidence angles.

To investigate further and quantify the effect of scale of the DTM data on the capability of this simulation to depict SAR distortions, we varied the resolution of the input elevation model from 90 m of the SRTM DSM, to 50 m, 10 m and 5 m of NEXTMap® DTM. Moving from 50 m to 10 m in the first instance, the results of the visibility simulation over the entire landmass show that modelled layover regions cover a total area of 3034 km^2 and 2996 km^2 in ascending and descending modes respectively (Table 1). These extensions show an overall increase from 1.0% to 1.3% of the total area of layover and shadow distortions across Great Britain (per mode) when moving from 50 m to 10 m data. Further change in the total area of simulated layover and shadow is found when moving to 5 m NEXTMap® DTM input data, with simulated layover and shadow for the entirety of the landmass reaching a total of 1.4% in each mode.

To analyse further this effect on the extension of the simulated distortions, in Fig. 6 we illustrate the results of the visibility maps in ascending mode for an area with moderately mountainous topography, i.e. the area of Lake and River Etive in Scotland (see location in Fig. 1). As expected, the input data resolution influences the results of the visibility maps, by increasing the level of detail with which the geometric distortions are identified and mapped. Moving from the SRTM to the NEXTMap® 5 m data we observe a decrease in the extent of foreshortening, from 25.8 to 25.1 km^2, an increase of layover from 13.1 to 14.1 km^2, and minor decrease of the areas of no distortions (i.e. 'good visibility'), from 22.7 to 22.4 km^2 (Fig. 7). Main areal differences seem to occur between the simulations using 50 m and 10 m resolution data, and it appears that by varying the input DTM resolution foreshortening and layover tend to change by following second order polynomials. Similar observations can be made by analysing the extension of layover and shadow regions for the entire landmass as modelled using the various input resolution DTMs (Fig. 8). Extrapolation to resolutions lower than 5 m (see dashed lines in Fig. 8a–b) seems to suggest that increased resolutions would bring the total extension of layover areas to ~3250–3300 km^2 in each mode, and ~1.8 km^2 shadow in ascending and ~7.6 km^2 in descending mode. Finer resolution DTM data (e.g., up to 25 cm LiDAR datasets) available at BGS for some test areas in Great Britain will help us to investigate this aspect further, though this analysis is beyond the scope of this paper.

Via validation with ERS-1/2 SAR data in South Wales (see Section 2.2.2) we show that in the case of medium resolution imagery, the use of the NEXTMap® DTM at 50 m resolution is suitable enough to model image distortions with a good degree of accuracy. This confirms that, although higher input resolutions such as 10 m obviously result in more detailed simulated distortions, the selection of the input elevation data needs to be a trade-off between higher DTM resolutions and respective cost of the data, and the NEXTMap® DTM at 50 m in our case provides an acceptable degree of accuracy.

2.2.4. Effect of variable incidence angles and ground track angles

As mentioned above, possible errors in the computation of the layover, shadow and foreshortening regions are thought to be due to a combination of:

(i) Use of a constant θ value across the entire image frame, without accounting for variations across the swath (e.g. from 19.2° to 26.7° for ASAR IS2 imagery; ESA (2007));
(ii) Use of a constant γ for the entire country, without accounting for variations with latitudes (e.g., in Great Britain, between 15.5° at the higher latitudes, i.e. 59°N, and 13.2° at 50°N); and
(iii) Potentially, major topographic changes occurring between the DTM reference date and acquisition of the analyzed radar imagery.

The first factor from the list above is considered to be the primary influence on the accuracy in our simulation. To support this statement, in Fig. 4d we summarize R-index changes for $\beta = 30°$ when θ varies from 19° to 43°. The various curves are all similar in shape and slightly parallel, showing peaks at $\alpha = +76°$ for the ascending and $\alpha = +284°$ for the descending modes, with R getting closer and closer to $+1$ with increasing θ. Although it is apparent that higher θ results in higher R-index and lower effects of active layover and foreshortening, it is worth noting that the effects of shadow are more accentuated when θ increases, i.e. when the LOS looks at the scene more obliquely, as further discussed below.

During our modelling over Great Britain we did not account for θ variations across the swath (cf. Section 2.2.1). For SAR sensors onboard ERS-1/2 and ENVISAT, θ across the swath varies between ~19° (near) and ~27° (far range). Hence more than 7° difference in the angle actually occurs from the near to the far range, and the hypothesis of a constant angle of 23° might be inappropriate for areas located away from the scene centre. In Fig. 4d it can be observed that R-index variations can be as high as ± 0.6 for fixed β and α, when moving from 19° to 27° θ.

To analyse further the influence of these variations across the swath of ERS and ENVISAT imagery and their impact on the resulting distortions, we simulated layover and shadow for the area of the River Etive in Scotland (~61.6 km^2 area; see location in Fig. 1), by varying θ from 19 to 27°. We also considered angles as high as 60°, in order to include a larger range of values which characterise other satellite sensors and may be analyzed for further discussion on the potential of other acquisition geometries. In Fig. 9 we show layover and shadow in ascending mode, which were simulated based on the 10 m NEXTMap® DTM, and by considering 14° γ. Whilst layover is most severe for small θ (e.g., near range), shadow effects are most severe when the θ is higher, and the LOS looks at the scene more obliquely (e.g., far range). For the area of interest, the extent of layover decreases drastically from ~19.2 km^2 (~31% of the area of interest) to 0.01 km^2 (i.e. ~0%) by increasing θ from 19° to 60°, with stronger decays observed for lower angles, e.g. around 50% drop off by moving from 19° to 27°. On the other hand, simulated shadows are null from 19° to 35°, then become significant at ~50°, and up to ~6.5 km^2 (i.e. 11% of the area of interest) by employing 60° θ.

Curves in Fig. 10 show that the differences in the simulated target areas affected by layover at the margins of an ERS or ENVISAT IS2 SAR scene (i.e. at 19° and 27° θ) can be as high as +8.5% (near) and −7% (far range) with respect to those estimated by employing a constant θ

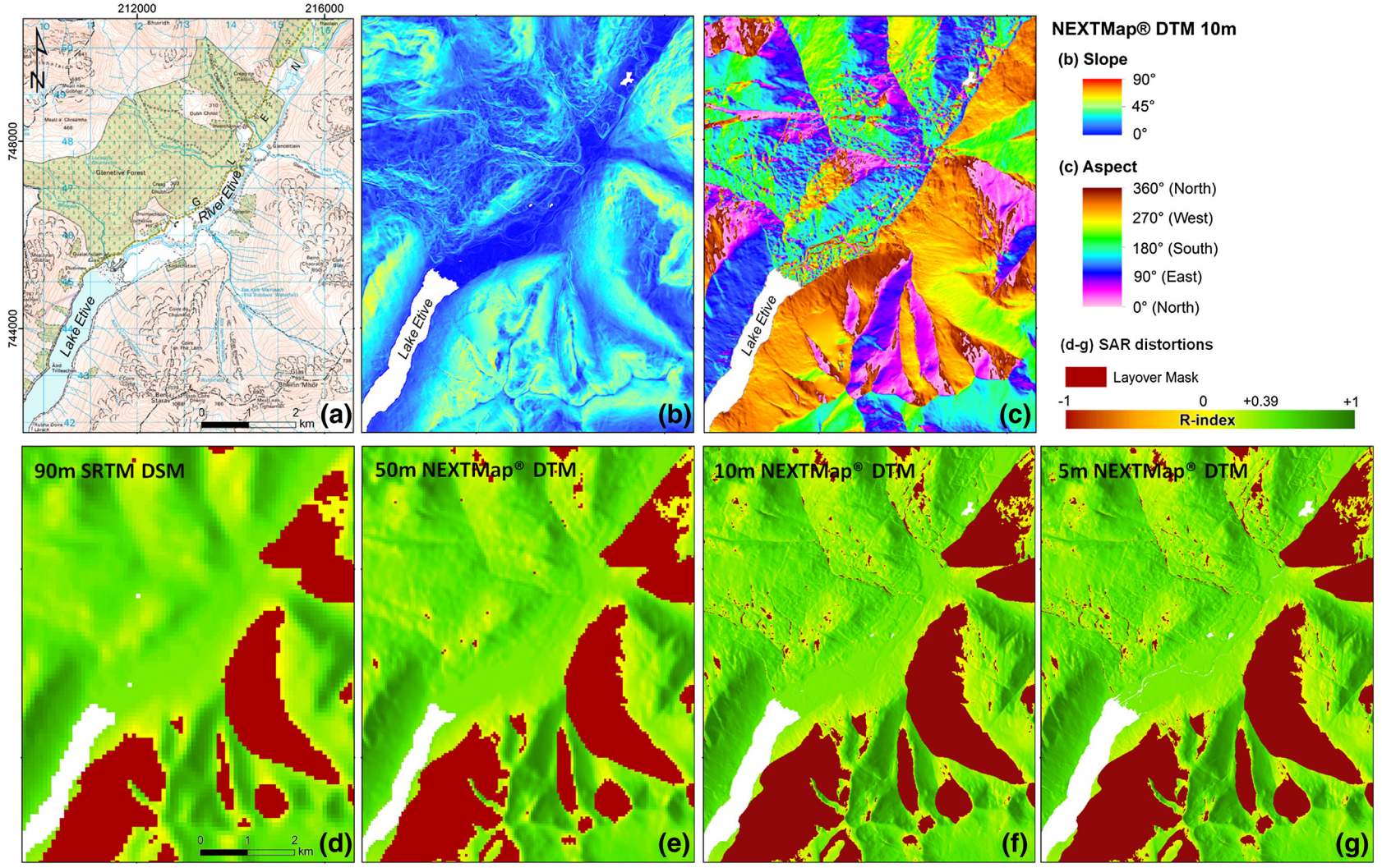

Fig. 6. (a) OS topographic map at 1:50,000 scale, terrain (b) slope and (c) aspect from the 10 m NEXTMap® DTM in the area of the Lake and River Etive, Scotland. Observed changes of the R-index and simulated layover regions in the ERS-1/2 and ENVISAT ascending mode with varying DTM resolution: (d) 90 m SRTM DSM, and (e) 50 m, (f) 10 m and (g) 5 m NEXTMap® DTM. Location of this area of interest is shown in Fig. 1b. Total areas of simulated distortions are summarized in Fig. 7. British National Grid; Projection: Transverse Mercator; Datum: OSGB 1936. OS data © Crown Copyright and database rights 2013. NEXTMap® Britain © 2003, Intermap Technologies Inc., All rights reserved.

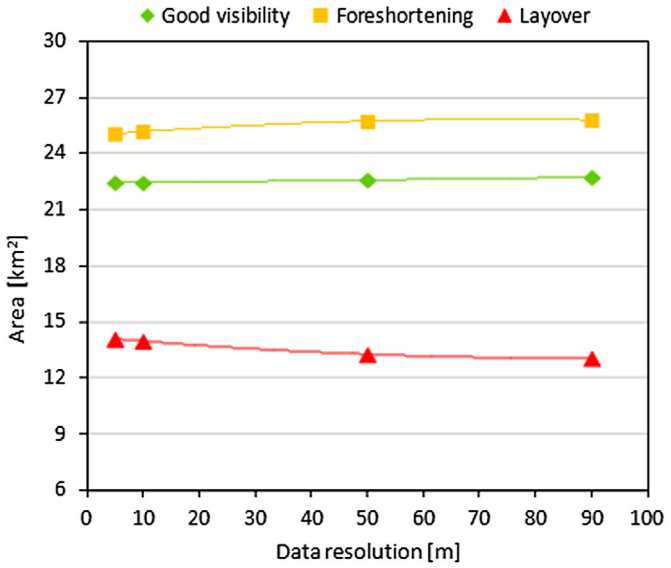

Fig. 7. Observed changes in the total areas of simulated SAR distortion in the ascending mode of ERS-1/2 and ENVISAT with varying DTM resolutions for the area of Lake and River Etive, Scotland. For each distortion, polynomial fits are overlapped onto observations. Refer to Figs. 1b and 6 respectively for the location of this area of interest and the map overview of simulated distortions.

of 23° across the entire frame. Analysed distortions seem to vary by following second order polynomial trends for both layover and shadow. These results allow us to draw the similar conclusions to those discussed by Gelautz et al. (1998), who simulated SAR data for a mountainous area in Oetztal (Austria) and observed decays of the simulated layover extent with respect to the analysed area from 30% to 6% and 1%, when moving from ERS-1/2 data with 23°, to JERS-1 data with 35°, to X-SAR data with 50° θ, and an increase from 0% to 1% and 6% of shadow respectively. Further insights into observed discrepancies due to θ variations across the swath are discussed during the validation in Wales (see Section 3).

In Fig. 4e we show that the effect of varying γ on the estimation of R is lower than that of other parameters, such as terrain β and LOS θ. Changes in γ cause shift of the R-index curves along the X-axis, hence the R values change for the various terrain α, with R peaks observed at $\alpha = 76°$ with 13° γ, 82° with 8° γ, and 60° with 20° γ. Aspect values for the peaks of the various curves are those characterising slopes parallel to the LOS, hence producing the best terrain visibility for that acquisition geometry. As also evident from the proximity of these curves, γ variations of 2.3° – i.e., the amount of γ change with latitudes across Great Britain – produce R-index differences as small as 0.01–0.05 for all possible α (i.e. 0 to 360°). We thereby believe that the impact of our assumption in this regard is of minor relevance.

The third factor, i.e. possible ground change occurred between the reference date of the DTM and acquisition of the analysed SAR image, represents clearly a potential source of error in the visibility maps, only if major movements of material and surface shape and volumetric changes occurred and have altered local topography to such a level that land changes are higher than the resolution of the input DTM and its vertical accuracy. In this case, the surveying of the modified territory becomes necessary to re-assess its local visibility to the satellite sensor. It is however beyond the scope of this paper to analyse this aspect further.

2.3. Land cover feasibility mapping and PS density prediction

The property of surface targets being 'Persistent Scatterers' is related to the terrain scattering properties that result in point-like signatures but not necessarily correspond to point-like objects (e.g., Nico et al., 2009). PS applications over the last decade have demonstrated that the identification of PS-like targets is controlled by interferometric coherence and phase stability and, in particular, a combination of the physical and geometric characteristics of the observed surfaces, the intrinsic properties of the radar signal, number and quality of input SAR images, and strategies and thresholds employed during the PS processing chain (e.g., Ferretti et al., 2001; Riddick et al., 2012). The first two factors mentioned above include the interaction between land cover and its variations through time, and the radar scattering process which mainly depends on the signal wavelength (e.g., 5.6 cm in C-band), terrain roughness, soil moisture and local incidence angles. The influence of input data and processing solutions mainly concerns the number and quality of SAR scenes used for the PS processing, the quality of the selected reference point, and the thresholds employed to identify PS candidates and final targets. The number of scenes controls also the accuracy of the estimated motions and velocities, and the possibility to detect (or not) radar targets on the ground, which in turn depends on the target persistence across the data stack, hence during the monitored interval.

Regarding land cover control, some authors have recently studied the correlation between PS locations and densities with respect to various land covers. Colombo et al. (2006) map the likelihood of identifying PS over different land use types and, similarly, Notti et al. (2010, 2011) synthesize the effects of land cover into the LU-index and combine it

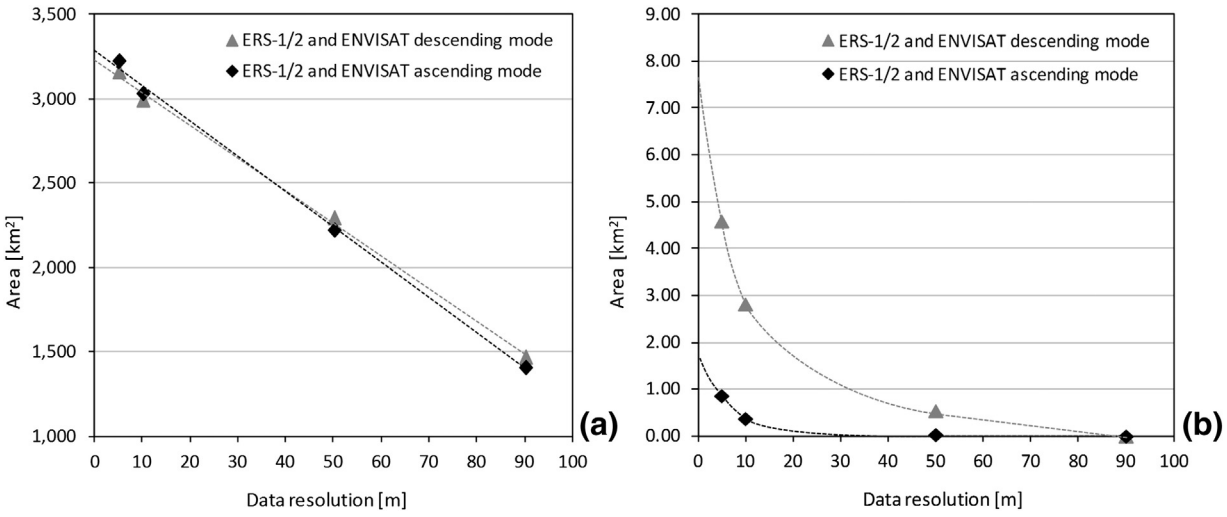

Fig. 8. Observed changes in the total areas of simulated SAR distortions in the ERS-1/2 and ENVISAT ascending and descending modes with varying DTM resolutions for the entirety of Great Britain: (a) layover; and (b) shadow.

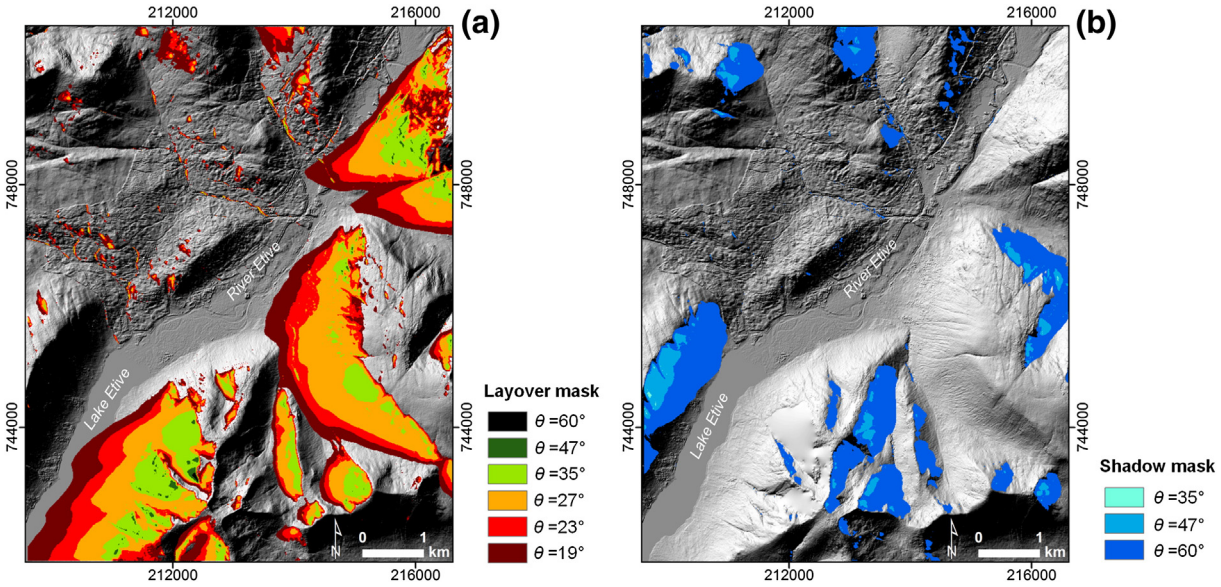

Fig. 9. Observed changes in the simulated (a) layover and (b) shadow regions in the ascending mode of ERS-1/2 and ENVISAT with incidence angles varying from 19° to 60° for the area of the Lake and River Etive in Scotland, overlapped onto 10 m NEXTMap® DTM shaded relief. Total areas of simulated distortions are summarized in Fig. 10. Location of this area of interest is shown in Fig. 1b. British National Grid; Projection: Transverse Mercator; Datum: OSGB 1936. NEXTMap® Britain © 2003, Intermap Technologies Inc., All rights reserved.

with topographic effects by deriving the RC-index by weighted averaging. More recently, Plank et al. (2013) developed empirical approaches for the estimation of the PS distribution prior to the processing and analysis of SAR data. These methods relate the number and distribution of PS targets to land cover and topographic data. Plank, Singer, Minet, and Thuro (2010) also rate the CORINE Land Cover 2000 (CLC2000) classes into 1 (very suitable) to 6 (not suitable) based on their suitability for InSAR analysis at the radar frequency bands L (~0.5–2 GHz), C (~4–8 GHz) and X (~8–12 GHz). Riddick et al. (2012) analyse the target selection process over various terrain types in the Cascades (Oregon, US) and correlate the location of ERS-1/2 PS to surface characteristics (e.g., roughness, bare earth exposure), geologic units, and vegetation density.

Notti et al. (2010) also observe that the PS density increases for higher R-index values. Similarly, Nico et al. (2009) study the variations of PS densities for various lithological units, and varying terrain slope and aspects in ideal InSAR conditions (i.e. absence of dense vegetation

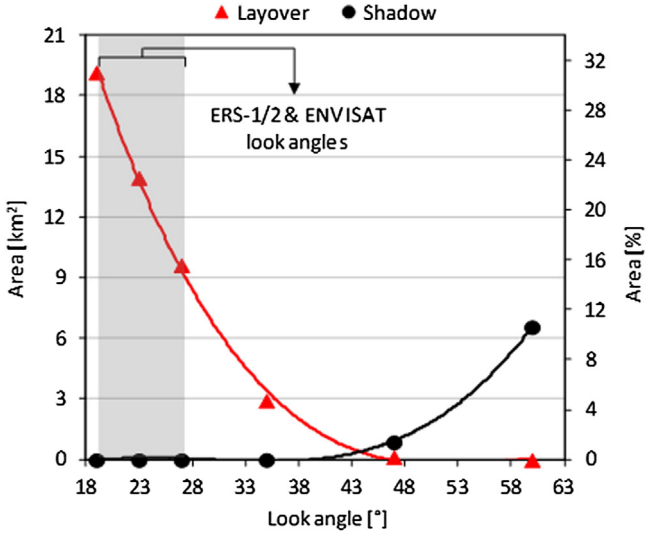

Fig. 10. Observed changes in the total area of simulated layover and shadow regions in the ascending mode of ERS-1/2 and ENVISAT with angles varying from 19° to 60° for the area of the Lake and River Etive, Scotland. Polynomial fits are overlapped onto observations for both layover and shadow distortions. Refer to Figs. 1b and 9 respectively for the location of this area of interest and the map overview of simulated distortions.

or other decorrelating factors). With regard to these latter studies, it is worth noting that the correlation between topographic factors (e.g., R-index) and the number of identified targets in hilly terrains is influenced by local variations of the ground range pixel size which are controlled, in turn, by local incidence angles. Slopes with very good visibility show that terrain orientation has little control on the success of InSAR analyses. In these cases, land cover and temporal decorrelation are thought to be the dominant factors determining the success of PSI- and SBAS-like techniques, as discussed in the following sections.

2.3.1. CORINE Land Cover 2006 calibration for Great Britain

Whilst other authors summarize the observations on PS distributions in different land cover types via dimensionless indices or classes irrespective of numerical calibration (e.g., Colombo et al., 2006; Notti et al., 2010), our study focusses on the exploitation of existing PS datasets for Great Britain as input data for the quantitative calibration of countrywide land cover data (Fig. 2). In this regard, our work builds upon the methodology presented by Plank et al. (2013) and, follows this up by employing a set of training areas in Great Britain to extend the pre-survey feasibility assessment to the entire landmass and land cover types mapped across the country.

The CORINE Land Cover map CLC2006 (EEA, 2007, 2012) was used as input land cover data for our assessment. The dataset has 100 m nominal accuracy and, for the UK, was generated based on the Land Cover Map 2007 (LCM2007; Morton et al., 2011). Of the 44 land cover types of CLC2006, 34 are mapped in Great Britain. Table 2 lists these 34 classes and shows the general predominance of non-irrigated arable land (CLC2006 code 211) and pastures (code 231) which cover more than 60,000 km^2 each, and moors and heathland (code 322) covering more than 20,000 km^2. Around 154,000 km^2 of sea and ocean cover is also mapped for a 25 km wide buffer area around the coastline of the main landmass and smaller islands and islets (see also Fig. 1a).

To provide a quantitative assessment of the likelihood of obtaining PS points for a given land use, we considered all PS data over British test sites available at the BGS (see Table 3). These datasets include geocoded PS data which were derived by Fugro NPA Ltd (now CGG, NPA Satellite Mapping Ltd) based on the Interferometric Point Target Analysis (IPTA; Werner, Wegmuller, Strozzi, & Wiesmann, 2003) and by TRE S.r.l. using the Permanent Scatterer InSAR (PSInSARTM; Ferretti et al., 2001) technique. These data were made available via the projects ESA Terrafirma and EC-FP7 PanGeo, and include a total of

Table 2
CLC2006 land cover types and their extension in Britain, calibration with existing PSI data, and validation of predicted PS densities with observed Point Target Candidates (PTC) densities in South Wales. Predicted PS/km^2 values are inferred for those land cover types with no values in the calibration area field. For the latter, the computation of the ratio between values of predicted (Pred.) and observed (Obs.) density values is not applicable (N/A). ρ, observed relative PS density with respect to CLC2006 class 112.

CLC2006 map			Calibration			Validation		
Code	Name	Total area in GB [km^2]	Area [km^2]	Observed* PS/km^2	ρ	Area [km^2]	Observed PTC/km^2	Ratio Pred./Obs.
111	Continuous urban fabric	279.6	96.6	836.5	2.02	3.9	156.9	5.3
112	Discontinuous urban fabric	12,192.9	1734.9	414.5	1.00	557.2	72.0	5.8
121	Industrial or commercial units	1683.8	188.6	392.2	0.95	95.0	66.7	5.9
122	Road and rail networks and associated land	103.7	17.6	218.1	0.53	1.5	35.1	6.2
123	Port areas	137.9	12.3	289.5	0.70	21.1	48.4	6.0
124	Airports	451.7	20.5	79.1	0.19	7.8	37.3	2.1
131	Mineral extraction sites	682.1	21.9	68.6	0.17	31.4	8.5	8.1
132	Dump sites	86.9	4.6	14.6	0.04	2.8	6.0	2.4
133	Construction sites	39.5	1.8	48.9	0.12	2.5	11.2	4.4
141	Green urban areas	639.8	165.4	149.0	0.36	11.6	30.3	4.9
142	Sport and leisure facilities	2695.8	227.3	54.5	0.13	72.3	7.0	7.8
211	Non-irrigated arable land	67,466.7	1184.0	32.2	0.08	1296.3	3.7	8.6
222	Fruit trees and berry plantations	16.7	0.8	3.2	0.01	–	–	N/A
231	Pastures	61,493.2	1440.7	31.4	0.08	3198.1	4.5	7.0
242	Complex cultivation patterns	209.5	0.0	35.0*	–	9.9	3.1	11.2
243	Land occupied by agric. and natural veget.	1346.9	29.2	38.3	0.09	73.2	3.8	10.2
311	Broad leaved forest	5282.9	170.8	25.0	0.06	280.8	5.3	4.7
312	Coniferous forest	13,011.4	20.8	10.7	0.03	554.8	1.5	7.1
313	Mixed forest	1423.7	10.0	29.5	0.07	23.8	4.7	6.3
321	Natural grasslands	18,260.0	1.7	59.8	0.14	973.8	3.1	19.0
322	Moors and heathland	22,174.2	3.2	19.0	0.05	305.8	5.0	3.8
324	Transitional woodland shrub	2873.1	9.0	9.5	0.02	96.1	1.6	6.1
331	Beaches dunes sands	460.2	1.2	38.2	0.09	13.9	10.1	3.8
332	Bare rocks	470.1	–	41.0*	–	–	–	N/A
333	Sparsely vegetated areas	4734.6	–	41.0*	–	–	–	N/A
411	Inland marshes	142.0	–	6.0*	–	12.4	0.3	18.6
412	Peat bogs	10,548.1	–	6.0*	–	65.8	2.1	2.9
421	Salt marshes	421.8	0.7	6.3	0.02	12.6	1.7	3.6
423	Intertidal flats	2667.8	6.7	91.5	0.22	98.4	4.1	22.5
511	Water courses	33.2	–	0.0*	–	–	–	N/A
512	Water bodies	1594.2	23.7	0.0**	–	12.8	0.9	0.0
521	Coastal lagoons	6.8	–	0.0*	–	–	–	N/A
522	Estuaries	258.5	2.2	0.0**	–	0.3	12.3	0.0
523	Sea and ocean	153,980.0	124.4	0.0**	–	2611.2	0.0	0.0

* = PS/km^2 values were inferred when too small or no calibration areas were available.
** = PS/km^2 values were reset to 0, by assuming no PS is found over water.

~2 M PS distributed over ~5700 km^2 land in England over the cities and surroundings of Greater London, Bristol, Bath, Stoke-on-Trent, and Newcastle and Durham (see Figs. 1 and 11).

For our feasibility assessment, the use of these input data was necessary to first derive the average PS densities which are observed for each land cover category in Britain when employing C-band, medium resolution SAR data (see also Fig. 2). To this aim, we averaged the observed densities of PS targets for the various land cover types for each PS data set in Table 3, by following the approach described by Plank et al. (2013). Within each PS dataset footprint, we computed the total number of targets lying within each CLC2006 class and then divided by the total area covered by the corresponding land cover type within the footprint. We subsequently combined the PS/km^2 statistics into an observed average across all six datasets with respective standard deviations, as summarized in Fig. 12a. This allowed us to extract relationships between the CLC2006 classes and the observed PS distributions in the six data processing results.

Differently from Plank et al. (2013) who used SAR data from X- and C-band sensors with different image modes, we did not need to apply any normalization to the PS densities, as only data with same wavelength, imaging mode, band and processing approach (both IPTA and PSInSAR™ belong to PSI-like methods) were employed for our

Table 3
ERS-1/2 and ENVISAT PS datasets used to calibrate the CORINE Land Cover map CLC2006 for Britain. Asc., Ascending; Desc., Descending; Coher., Coherence.

ID	Satellite	Orbit	No. of scenes	Dates	No. of PS	Min coher.	Processed area [km^2]	Site(s)	PS provider & reference project
1	ERS-1/2	Asc.	27	19/06/1992–31/07/2000	727,939	0.53	2537	London	CGG, NPA Satellite Mapping Ltd, EC-FP7 PanGeo
2	ENVISAT	Desc.	45	13/12/2002–17/09/2010	835,539	0.49	2394	London	CGG, NPA Satellite Mapping Ltd, EC-FP7 PanGeo
3	ERS-1/2 and ENVISAT	Desc.	75	11/05/1992–27/01/2005	60,147	0.25	1131	Bristol, Bath	CGG, NPA Satellite Mapping Ltd, ESA Terrafirma
4	ERS-1/2	Desc.	70	11/05/1992–27/02/2003	142,771	0.56	1125	Stoke-on-Trent	TeleRilevamento Europa (TRE) Srl, ESA Terrafirma
5	ERS-1/2	Desc.	48	19/04/1995–14/12/2000	114,857	0.57	978	Newcastle, Durham	CGG, NPA Satellite Mapping Ltd, ESA Terrafirma
6	ENVISAT	Desc.	21	03/12/2002–07/10/2008	71,462	0.75	978	Newcastle, Durham	CGG, NPA Satellite Mapping Ltd, ESA Terrafirma

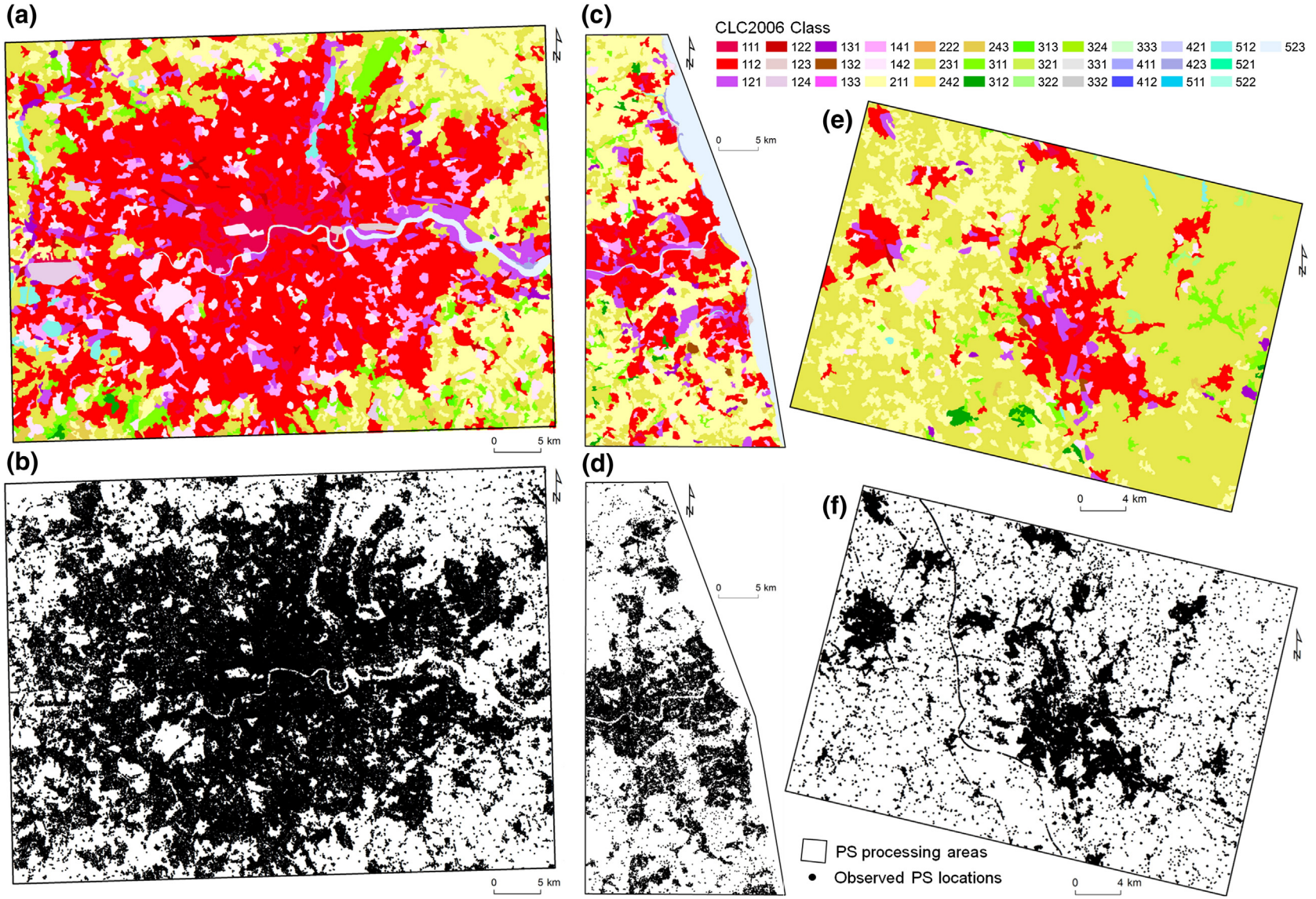

Fig. 11. Examples of CLC2006 map and distribution of ERS-1/2 PS targets for the calibration datasets in (a–b) Greater London, (c–d) Newcastle–Durham, and (e–f) Stoke-on-Trent. Reference IDs of the datasets with respect to Table 3 are (1), (5) and (4), respectively. Location of the sites is represented in Fig. 1a. CLC2006 classes associated with legend codes are summarized in Table 2. British National Grid; Projection: Transverse Mercator; Datum: OSGB 1936. CLC2006 © 2007, European Environment Agency (EEA). ERS-1/2 PS data in (b) © CGG, NPA Satellite Mapping Ltd; ERS-1/2 PS data in (d) and (f) © European Space Agency.

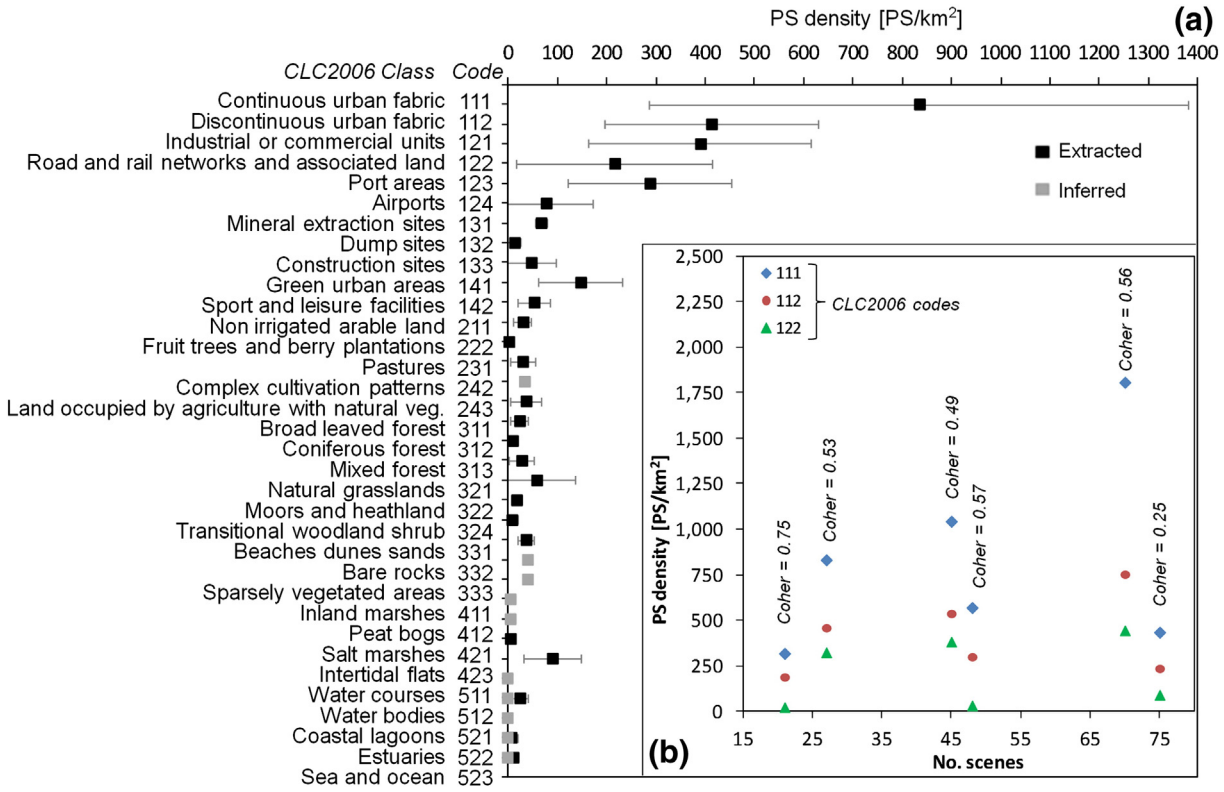

Fig. 12. (a) Average and standard deviation of PS densities estimated using the four calibration sites for the 34 CLC2006 classes mapped in Great Britain; and (b) variations of the PS densities against the number of the processed scenes for the six calibration stacks and three land cover types. Refer to Table 2 for statistics observed for the CLC2006 classes.

calibration. Climate conditions are similar in the four calibration sites (Met Office, 2013a), therefore no initial climate classification and compensation were performed.

It is worth noting that, prior to the computation of the average PS densities and other statistics for the various land cover types, we first masked the CLC2006 by using the layover and shadow masks generated by following the methodology described in Section 2.2 (see also Fig. 2). This allowed us to discard regions not visible to that particular acquisition mode (e.g., descending for the ERS data for Stoke-On-Trent). Within these areas, indeed, the lack of PS targets is due to geometrical constraints but is not necessarily land cover-related. Inclusion of these areas within the computation of the PS density statistics would have caused an erroneous decrease of the computed densities. Layover and shadow for our calibration sites were, in this case, quite small with respect to the total calibration area, i.e., only ~2 km^2 in total over the four sites (half of which were mapped at the outskirts of Bristol and Bath), which represent less than 0.1% of the total extension of the land areas used for calibration, i.e. ~5700 km^2. Thus their removal had minimal impact on the estimation of the statistics.

Fig. 12a shows the different target densities observed (black squares) or inferred (grey squares) for the 34 land cover types of Britain. Inferred values were adopted when no polygons of those particular land cover type were sampled by the available PS input datasets. These include the following seven types: bare rocks, sparsely vegetated areas, inland marshes, peat bogs, complex cultivation patterns, water courses and coastal lagoons. The absence of these CLC2006 classes in the calibration sites suggested that the mapped land cover in these PS datasets was not fully representative of the entire range of land covers present in Great Britain, as further revealed during the validation in Wales (see Section 3). For these types, the potential PS densities were attributed based on similarities with other land cover types (see also Table 3). Values over water bodies, estuaries and sea and ocean were set to zero by assuming the absence of PS targets in areas covered by water.

The land cover types were sorted according to their observed or inferred PS densities, and catalogued into nine density classes: (Class 9) 0 PS/km^2; (Class 8) 0–10 PS/km^2; (Class 7) 10–20 PS/km^2; (Class 6) 20–40 PS/km^2; (Class 5) 40–80 PS/km^2; (Class 4) 80–160 PS/km^2; (Class 3) 160–320 PS/km^2; (Class 2) 320–640 PS/km^2; and (Class 1) with a density of >640 PS/km^2.

2.3.2. PS density observations and comparative analysis with external studies

Observed target densities over the calibration sites show that surface objects with higher temporal phase stability result generally in PS densities as high as several hundreds of scatterers per square kilometre (Fig. 12a). Typically, urban and built-up areas result in higher PS density than rural areas and, for instance, discontinuous urban fabric and industrial or commercial units (i.e. CLC2006 codes 112 and 121) show average densities of ~400 PS/km^2, with ±200 PS/km^2 deviation across the six input PS datasets, whilst non-irrigated land shows observed densities of ~32 ± 17 PS/km^2.

In accordance with our findings for the calibration sites, Colombo et al. (2006) observed comparable PS densities for the various classes, e.g., up to ~1160 PS/km^2 for infrastructure, ~290 PS/km^2 for bare rocks, ~110 PS/km^2 for grassland and ~30 PS/km^2 for grass, lawn, and forests, based on one set of PSInSAR™ ERS-1/2 data available over Piedmont (Italy). Tapete and Cigna (2012) observe ERS-1/2 and ENVISAT average densities from 75 to 290 PS/km^2 for the rural, moderately vegetated site of Bivigliano (Italy). Rodriguez Gonzalez, Adam, Parizzi, and Brcic (2013) observe peaks of 200 ERS-1/2 PS/km^2 over the urban area of Athens for their WAP InSAR results in Greece.

We noticed that, although the majority of land cover types typically show consistent densities across the calibration sites and very little or moderate standard deviations (Fig. 12a), higher variability is found for continuous and discontinuous urban fabric (codes 111 and 112), industrial and commercial units (code 121), road and rail networks (code

122), port and airport areas (codes 123 and 124) compared to natural and vegetated and other land cover types. For instance, CLC2006 type 111 reveals the highest variability across the six datasets, with up to ±545 PS/km^2 observed. High values for the observed standard deviations relating to urban land cover types agree with observations by Plank et al. (2013) for other sites with different climatic and environmental settings in Central Europe.

To further investigate this variability, we analyzed the PS density variations across the six datasets with respect to the input number of SAR scenes and employed thresholds to select the final set of PS targets. Results of this comparison are shown for the CLC2006 types 111, 112 and 122 in Fig. 12b. This plot highlights the existence of moderate correlation between the observed densities and the number of scenes composing the datasets with, typically, higher numbers of input images resulting in higher PS densities. Significant variations are observed, however, across the six datasets which seem to be part controlled by the coherence thresholds used by the PS providers before the delivery of the datasets. Indeed, for the five datasets processed by the same provider (hence with the exception of the dataset available for Stoke-on-Trent; see Table 3), it is apparent that for stacks with similar numbers of scenes (for instance, the ENVISAT dataset for London, and the ERS dataset for Newcastle, with 45 and 48 scenes respectively), the lower the coherence threshold, the greater the number of targets included in the corresponding dataset (Fig. 12b).

Through our validation in South Wales (see Section 3) we show that, despite the variations induced by the input number of scenes and coherence thresholds, the relationships and rankings of the various land cover types stay the same across the entire processed scene. Hence these parameters influence the numeric value of the number and density of identified targets, but not the density proportions between the different land cover types. This confirms what was discussed by Plank et al. (2013) regarding 'relative PS densities' between the various land cover classes.

Our observations for the calibration sites also agree with the land cover rankings proposed by Plank et al. (2010) for the CLC2000, with highest densities found for the topmost classes proposed by these authors. Exceptions are airport areas (code 124) which appear to provide lower density based on our calibration in Britain, and intertidal flats (code 423) where the calibration shows moderately high rather than the lowest density ranking. These results are discussed and clarified via the validation in Wales (see Section 3).

2.3.3. Land cover-derived PS densities for Great Britain

We used the observed PS densities from our calibration (see Table 2) to extend the assessment to the ~230,000 km^2 total area of the landmass to predict where PSI-like techniques are most likely to succeed and where not, and PS targets to be or not identified (Fig. 13).

PS density statistics extended over Britain confirm that land cover has stronger control on the potential and success of these techniques over this mostly vegetated land (see also Fig. 1) than local topography (see Section 2.2.2). The most represented PS density class in Britain is class 6 (i.e. 20–40 PS/km^2), covering an area of more than 137,000 km^2 across most of England and Wales, and part of southern/eastern Scotland (Fig. 13). This class includes pastures, complex cultivation patterns, land occupied by agriculture with areas of natural vegetation, broad leaved and mixed forest, beaches, dunes and sands. Class 7 (i.e. 10–20 PS/km^2) shows an extension of more than 35,000 km^2 and is mainly found in the northern counties, in Scotland and northern England, and part in Wales, where moors, heathland, and coniferous forest are mapped. Classes 1 (i.e. >640 PS/km^2) to 4 (i.e. 80–160 PS/km^2) concentrate over the major cities and towns of Britain, with largest occurrences in Greater London, Birmingham, Manchester and Glasgow. In general, lowest potential for PS studies is found in Scotland, where classes 5 to 8 dominate.

By accounting for the extension of all CLC2006 polygons across Britain and the calibrated PS densities, the overall number of monitoring targets that might be identified over the entire landmass for each acquisition mode (ascending or descending) exceeds 12.8 M. This prediction refers to the use of a PS approach (hence not coherence based, multi-look methods such as SBAS) with C-band ERS-1/2 or ENVISAT medium resolution data. This would correspond, on average, to a density of ~55 PS/km^2 for the entire landmass, which reflects the predominance of PS density classes 5–6. Similar to our numerical prediction is the density observed by Rodriguez Gonzalez et al. (2013) who found more than 1 M PS over a ~65,000 km^2 total processed area in Greece with their ERS-1/2 InSAR analysis, with overall average density of ~16 PS/km^2. The latter reveals average densities lower than those we have predicted over predominantly agricultural and rural areas of Britain, and seem to reflect the predominance of forests and semi-natural areas for the territory in Greece processed by these authors. Further insights into this aspect are revealed by the validation in Wales (see Section 3).

The calibrated CLC2006 map in Fig. 13 clearly has to also account for the various geometric distortions and, in particular, by masking out active and passive layover and shadow regions (see Section 2.2.1) from the predicted PS density map in order to remove areas where topography prevents any target to be imaged by the radar sensor. This is discussed in Section 4, which illustrates how to use these feasibility maps for SAR-based landslide studies.

3. Validation in South Wales with ERS-1/2 SAR imagery

To validate the simulated distortion maps and the calibrated CLC2006 map, by using the GAMMA software and the IPTA approach we processed a stack of 55 ERS-1/2 SAR scenes acquired between 1992 and 1999 in South Wales in descending mode along satellite track 409 (Fig. 14). The number of scenes composing this stack is representative of the typical number of images constituting ERS-1/2 descending mode stacks over Great Britain, which generally have over 50 scenes (see Fig. 3 and Section 2.1). Furthermore, the imaged area of interest samples the various land cover types observed over the landmass (Figs. 15a–b and 1), with not only urban fabric but also extensive rural areas, thus providing large representation of non urban areas of Britain.

Orbit state vectors for the ERS-1/2 images were first improved by employing the recomputed orbital data provided by the Delft Institute for Earth-Oriented Space research (DEOS), made available via ESA's project REAPER (REprocessing of Altimeter Products for ERS) in 2011. The stack was then co-registered to a single master scene acquired on 25/09/1995, obtaining co-registration accuracies for the slave scenes up to 0.05 pixels in range and 0.15 in azimuth.

In Fig. 14 we show the SAR intensity of the ERS-2 scene acquired on 14/12/1999, which was multi-looked with 1:5 look factors in range and azimuth and geocoded to the 50 m NEXTMap® geometry, with final resolution of 50 m to be consistent with the DTM. Regions of layover and shadow were identified within the scene during the radar-to-map transformation. Observed SAR distortions over an ~7000 km^2 area of land (South Wales only) were compared to the simulated distortions to assess the accuracy of the simulation. Distortions across the scene cover around 1% of the validation area, which is similar to the amount of distortions simulated for the entirety of the landmass (see Section 2.2.2). This confirms further the good representativeness of this test site to perform validation in our study.

Validation in Wales shows that the use of the 50 m NEXTMap® DTM for the layover simulation results in discrepancies with the actual layover by ~11% of the total layover identified across the ERS scene, with simulated regions covering 107 km^2 (hence 1.5% of the processed area) and those observed in the ERS scene covering 97 km^2 (hence 1.4% of the processed area). This suggests that, over the entirety of the landmass, the extension of simulated layover regions in each satellite mode needs to be adjusted (in particular, decreased) to account for the 11% discrepancy, and this brings to around 0.9% of our estimation based on the 50 m DTM input dataset and, analogously, to 1.2% and 1.3% of the estimates based on the 10 m and 5 m DTMs.

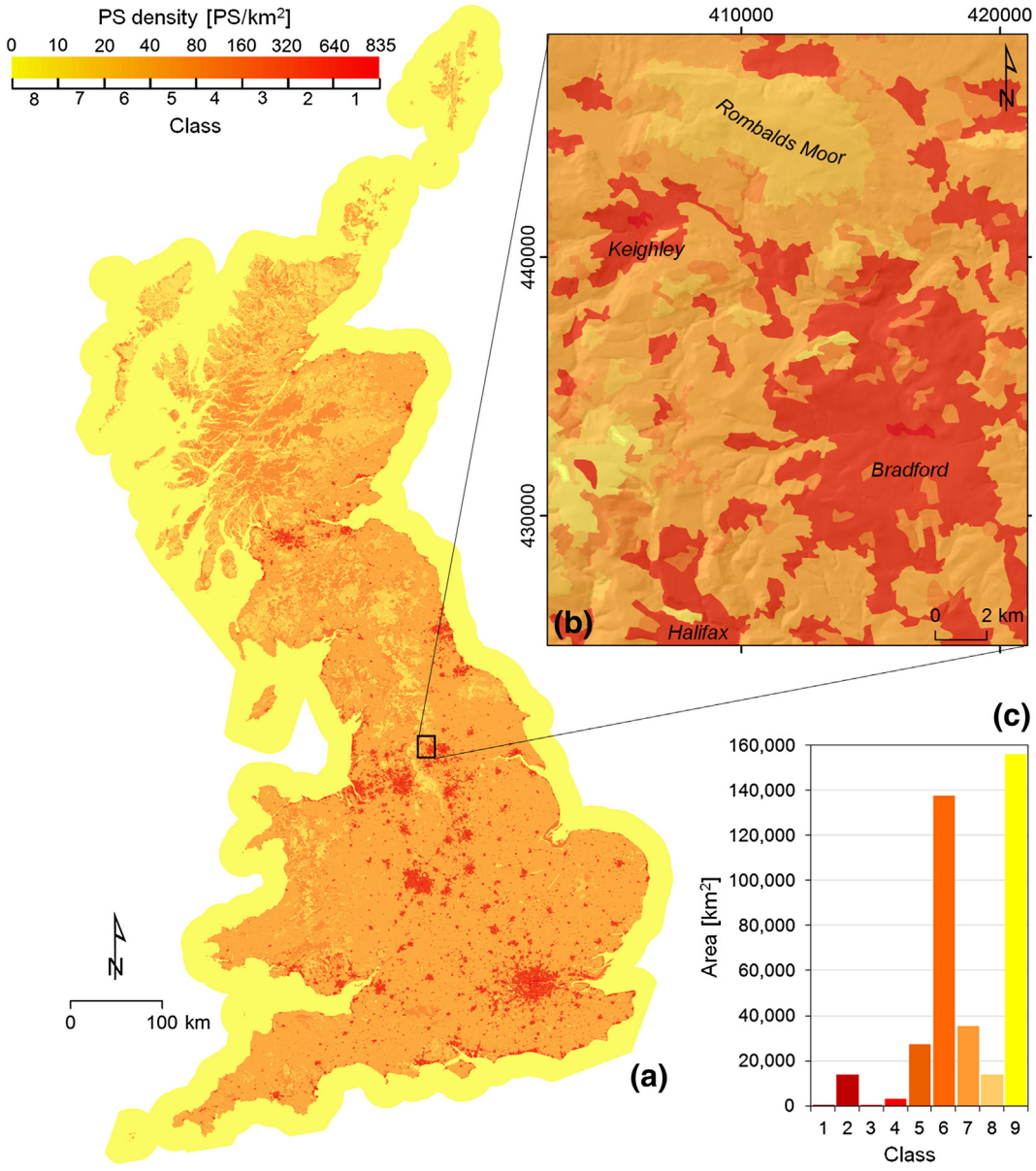

Fig. 13. Calibrated CLC2006 indicating PS density classes for Great Britain (a) and example for the area of Bradford, England (b). Histogram (c) shows total area statistics of (a) for the nine CLC2006 classes identified based on PS density observations for the four calibration sites. Full reference to the nine PS density classes is provided in Section 2.3.1. British National Grid; Projection: Transverse Mercator; Datum: OSGB 1936.

Simulated layover in the near range (i.e. to the east, in the descending scene) shows smaller extensions than areas of observed layover, likely due to the use of the constant θ (23°) that, in the near range, results in lower distortions compared to those caused by the actual θ of the near range, hence ~19° (see Figs. 14e–f, 4d and Section 2.2.2). On the other hand, in the far range (i.e., to the west) the simulated layover regions are more extended than those observed in the ERS scene, as an effect of a larger θ used to model distortions with respect to the actual value in the far range (see Fig. 14a–b). Analysis of layover regions in the mid range, where the θ value employed for the simulation is closer to that observed (~23°), the discrepancies between modelled and observed layover areas minimise to only 5% in total (see Fig. 14c–d). The latter is obtained as average over an 11 km wide elongated test area of ~900 km^2 running along the mid range of the ERS image.

To validate the calibrated CLC2006 map, we used IPTA and exploited the amplitude dispersion criterion to identify a set of radar targets showing low temporal variability of their SAR intensity values across the entire stack, by setting a threshold for the ratio between average and standard deviation of the backscattering of 1.5, and focussing only on points dominating the radar echo of the image. The latter condition was implemented by selecting only point targets showing intensities higher than the spatial average, which allowed masking out points within areas of radar shadow, i.e. of low backscattering.

The generated set of Point Target Candidates (PTC) was geocoded to the map geometry based on the NEXTMap® DTM at 50 m resolution. The dataset includes ~77,100 points within the full frame (100 by 100 km), which are distributed mainly along the southern coast of Wales over the urban areas of Swansea and Cardiff and, to the north, over smaller villages and towns built in the narrow valleys of the South Wales Coalfield (Fig. 15c). Average target densities for the entire frame over areas of land (~7800 km^2; i.e., by masking out the Bristol Channel water area) are ~9.9 PTC/km^2, whilst peaks of 200–240 PTC/km^2 are found for the urbanised areas. Lowest densities are observed to the north, where there are natural grassland and pastures.

Validation of the CLC2006 calibrated map was based on comparison of the PS density predictions with the observed PTC densities within

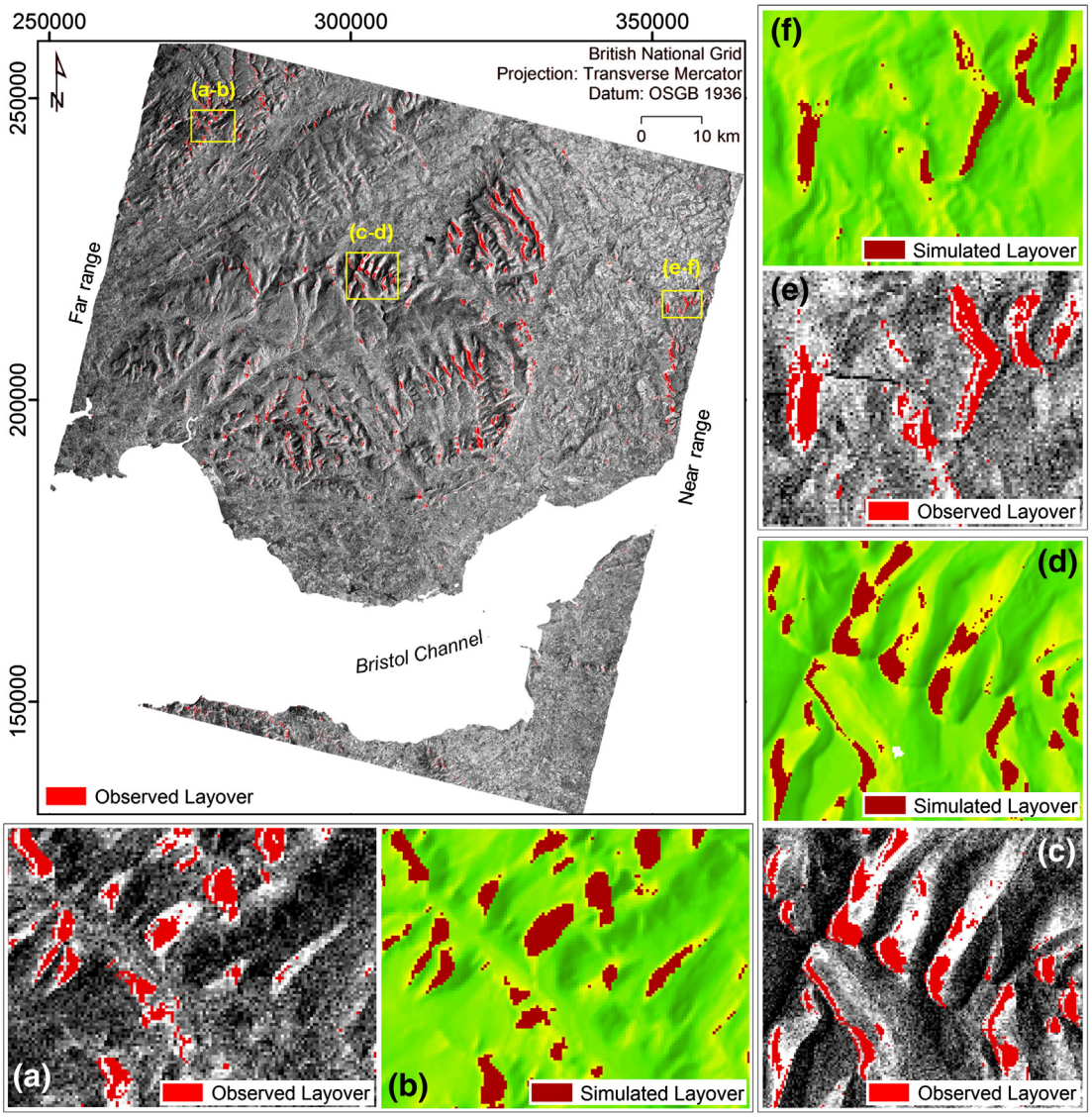

Fig. 14. Geocoded and multi-looked intensity image (1 × 5 look factors) of the ERS-2 SAR scene (14/12/1999) in descending mode. (a,c,e) Observed and (b,d,f) simulated radar layover regions in South Wales in the far (a,b), mid (c,d) and near (e,f) range based on NEXTMap® 50 m DTM data. Location of this area of interest is shown in Fig. 1b.

each land cover type. There are 2565 CLC2006 polygons within the South Wales ERS data frame. To extract values for the observed densities for these polygons, we first masked the map by removing layover regions, which in this area have non-negligible extension (i.e. ~100 km^2).

Results of the validation are summarized in Fig. 15b–c, where the predicted PS densities are compared with the observed PTC locations. Visual comparison of the maps confirms that the highest PTC densities are found for CLC2006 polygons with higher PS predictions, and there is very good match between land cover rankings of our predictions with respect to observed PTC densities. Numerical comparison is also represented via the scatterplot in Fig. 15d, which shows that predicted densities are on average 5 times higher than those observed, but this ratio remains constant throughout all land cover types, as shown by the very high R^2 coefficient of the linear regression applied to the data, i.e. 0.96. In other words, although the absolute differences between predicted and observed densities are clearly significant, the general relationship between the densities observed for the various land cover classes is largely similar, hence the land cover rankings are confirmed on the whole, despite differences in the algorithms and thresholds which were employed for the calibration sites. This aspect was accounted for to adjust our predictions across the landmass, and the total number of PS predicted for Great Britain (i.e. 12.8 M; see Section 2.3.1) was therefore rescaled by using this factor, thus obtaining a rescaled potential for over 2.5 M monitoring targets across the landmass.

Our observation for the land cover relative relationships agrees with what Plank et al. (2013) observed, as well as with their concept of 'relative PS densities', which refers all target densities to a reference land cover class (e.g., discontinuous urban fabric), to which all other types are relative. These relative PS densities are found fairly constant across the various PS datasets and can be used as a reference to assess the spatial distribution of targets prior to a PS analysis based on the CLC2006 map. The results of the relative densities computation for our six calibration datasets of Britain are summarized in Table 2 and mostly confirm those observed by Plank et al. (2013) in central and eastern Europe by using other PS data sets derived using ERS, ENVISAT, RADARSAT and TerraSAR-X SAR data.

3.1. Observed PS density outliers

The predicted PS densities for a few land cover types overestimate those observed by factors higher than 5, which is shown by points

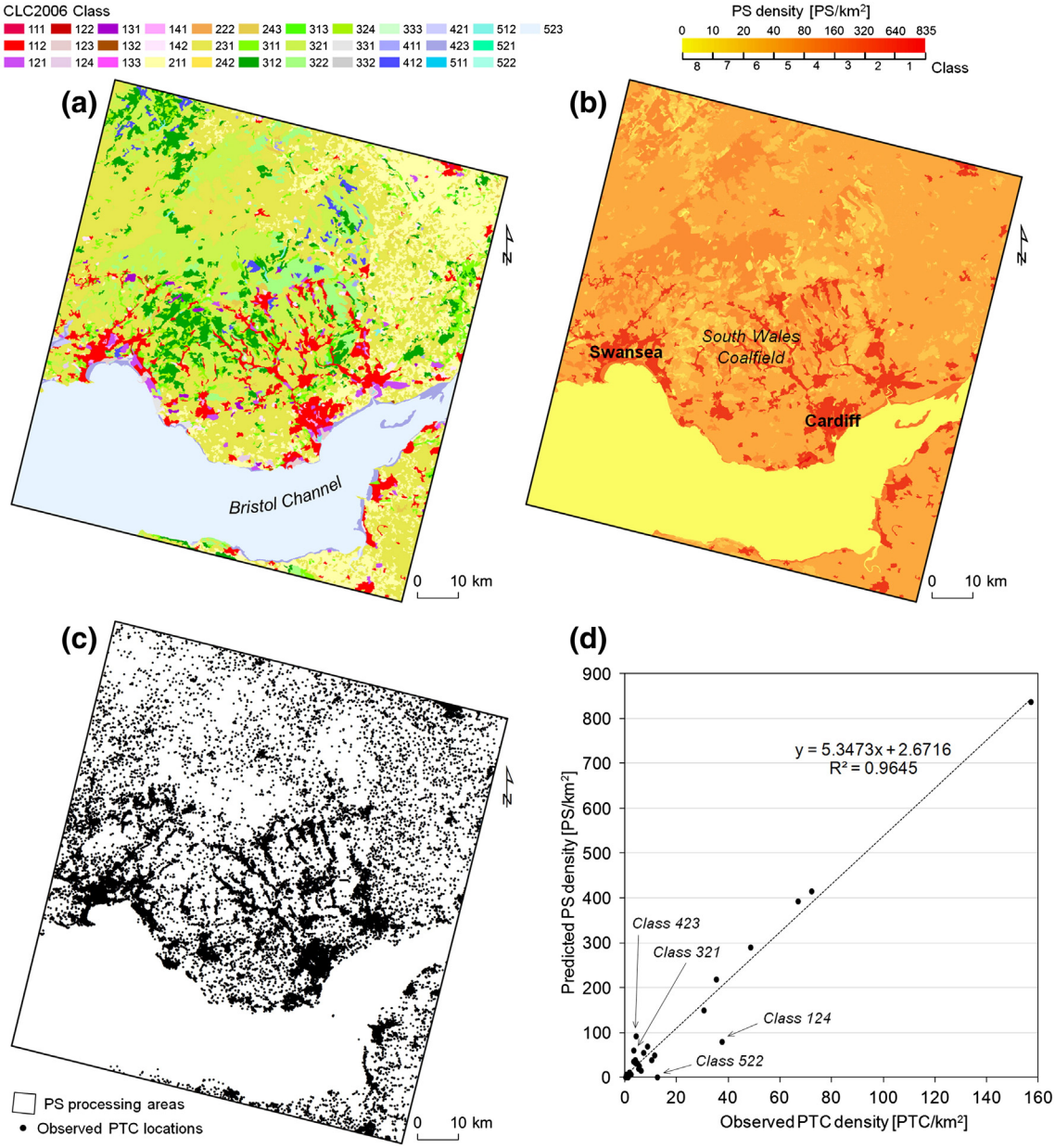

Fig. 15. (a) CLC2006 map, (b) predicted PS densities and (c) observed PTC densities for a full ERS-1/2 frame acquired in descending mode over South Wales. Scatterplot (d) compares predicted with observed densities for each CLC2006 land cover type. CLC2006 classes associated with legend codes are summarized in Table 2. Location of this area of interest is shown in Fig. 1b. British National Grid; Projection: Transverse Mercator; Datum: OSGB 1936. CLC2006 © 2007, European Environment Agency (EEA).

above the linear trend line in the scatterplot shown in Fig. 15d. Discrepancies are found for areas covered by natural grassland (~60 PS/km^2 vs. ~3 PTC/km^2) and intertidal flats (~92 PS/km^2 vs. ~4 PTC/km^2). This can be explained by comparing the extent of the CLC2006 polygon areas used for calibration and those found within the ERS frame for South Wales. Predictions for natural grasslands, for instance, are based on CLC2006 polygon areas of only ~1.7 km^2 (found in Newcastle and Stoke-On-Trent datasets only), and thus not very robust due to the small extent of the calibration areas. On the other hand, the natural grassland polygon area in Wales is 973 km^2, and thus considered more robust than the calibration value. Similarly, the PS density values for intertidal flats are based on 98 km^2 in Wales and 7 km^2 in the calibration sites, hence the density value for this land cover type has lower degree of robustness. We conclude that the densities for these land cover types were not represented well by the calibration datasets.

PTC density values found for inland marshes (~0.3 PTC/km^2) are based on polygon areas of 12 km^2 in Wales, but find no correspondence in any calibration statistics due to the absence of this class within the areas used for the calibration, and the consequent need to infer a density value for this land cover (see Table 2). Other similar examples are the lack of PS input data over areas of peat bogs and complex cultivation patterns and need to arbitrarily assign PS density rates during the CLC2006 data calibration. Although the exploitation of the average ratio between predicted and observed values (i.e. ~5) could, in principle, increase the observed values for inland marshes and peat bogs to ~1.5 PS/km^2 and ~10 PS/km^2 respectively, to compare them with our inferences, these would still fall within the PS density class 8, for which densities are generally lower than 10 PS/km^2. Whereas exploitation of the ratio for complex cultivation patterns would move this type from class 6 to 7 (i.e., ~15 PS/km^2).

Another exception to the linear regression in Fig. 15d occurs for airport areas (code 124), for which predicted densities are only two times higher than those observed during the validation. This suggests that either the calibration for this class provided too low PS density statistics,

or the validation provided much higher statistics. In principle, the estimation of the average density for this land cover type during the calibration was considered more robust due to the wider representation of this land cover within the calibration sites, since a total of ~20.5 km^2 was used during the calibration whilst only 7.8 km^2 was present in Wales. In this case, however, observations by other authors (Plank et al., 2010) suggest that this class should belong to classes with PS densities higher than what we observed. By projecting the value of the PTC density of Wales using the average ratio of 5, we obtain ~187 PS/km^2, and this would correspond very well with observations by the above cited authors, and therefore suggests possible presence of other sources of errors within the input layers. We identified a source of error in the difference in the resolution and scale of the input CLC2006 and PS data. Indeed, the identification of land cover types is made at a different scale with respect to point-wise locations of the PS input datasets and it may occur – especially at the margins of two or more CLC2006 polygons – that PS targets belonging to a certain land cover class fall into another polygon due to the higher scale (lower resolution) of the CLC2006 data. Evidence of this was found for airport areas within the calibration sites.

To address the above, future improvement of our calibrated PS density map will therefore be investigated based on higher resolution land cover data of the LCM2007 produced by CEH-NERC (Morton et al., 2011), or the Copernicus (formerly GMES) Urban Atlas (EC, 2011).

4. Use of InSAR feasibility maps for landslide research in Great Britain

The feasibility maps that we have generated via the methodology discussed in Sections 2.2 and 2.3 can be used to guide selection of best data stacks and datasets to monitor the different areas of Britain. Indeed, various recommendations and information can be revealed by using the results of our feasibility assessment before a SAR-based study and processing of radar stacks start, among which, for instance:

(i) Mapping of the location of SAR layover and shadow region based on a given acquisition geometry (i.e., LOS θ and γ) before the acquisition of new SAR imagery or selection of data from existing SAR archives;
(ii) Identification of the best acquisition geometry (e.g., best θ) and mode (e.g., ascending/descending orbit) to guarantee good visibility of target areas;
(iii) Quantification of the fraction of maximum slope-oriented motions measurable along the satellite LOS (by using the R-index for areas of good visibility or foreshortening); and
(iv) Understanding where PS points are likely to be identified, and which land cover types will produce higher and lower densities of persistent targets.

Regarding the third point above, recent publications have sought to quantify the percentage of slope-oriented motions that the satellite LOS can estimate (e.g., Barboux et al., 2011; Cigna, Bianchini, et al., 2013; Herrera et al., 2013; Notti et al., 2011; Plank et al., 2012). The calculation of this percentage is based on geometrical considerations analogous to those behind the R-index and, for areas of good visibility or foreshortening, corresponds with the R-index value. Clearly, the significance of this factor is null for areas of layover or shadow, where no information about land motion can be retrieved by using SAR data. Moreover, the validity of the assumption of maximum-slope oriented motions is limited to hilly and mountain areas and some types of landsliding and gravity-controlled processes, whereas for flat areas and very gentle slopes the use of this conversion has no significance.

In addition to information relating to existing image archives, our feasibility assessment supports the selection of the acquisition modes of new satellite SAR missions (e.g., Sentinel-1 constellation), via a priori (i.e. pre-survey) simulation of SAR geometric distortions based on various LOS orientations, and prediction of radar target densities and distributions based on land cover. Thus, the replication of our feasibility assessment to account for the acquisition modes of new Earth explorers such as Sentinel-1 is going to clarify their potential to image Great Britain in the near future.

By exploiting the results of our research, we have analysed the feasibility of InSAR to monitor various areas of Great Britain, with particular regard to landsliding processes. As anticipated in Section 2.2, to assess the feasibility of a SAR-based study, in particular when dealing with unstable slopes, the success of any analysis based on SAR imagery is controlled by the sensor acquisition geometry and the presence of image distortions. For these areas, the visibility to a certain satellite mode can vary within the different portions of the same slope, based on local terrain orientation.

The most extensive sources of information on landslides in Great Britain are the National Landslide Database (NLD) and the mass movement layer of the Digital Geological Map of Great Britain (DiGMapGB), which were produced and are maintained by BGS. The NDL documents the location, name, dimensions, type, trigger, damage caused and references for more than 15,000 landslide point-wise records which are, since the late 1980s, regularly updated by the BGS Landslide Response Team as new information becomes available or events occur (Foster, Pennington, Culshaw, & Lawrie, 2012). The mass movement layer of the DiGMapGB at various scales incorporates the outline of landslide deposits that have been recorded and mapped by geologists in the field (Smith, 2013a, 2013b).

DiGMapGB and NLD data are being compared with the feasibility maps and show that the dominant factor controlling the application of InSAR techniques over regions affected by landsliding in Great Britain is land cover. Indeed, whilst the mutual use of ascending and descending modes mostly compensates the issues related to SAR distortions in each acquisition mode, areas affected by landslides generally have extremely to very low potential for PS-like analyses. Cigna, Bateson, Jordan, and Dashwood (2013) discussed preliminary results of the assessment for the area of Manchester and the Peak District in central/northern England. For this region, the visibility of some areas of landslide deposits which are mapped in the DiGMapGB and the NLD in the area of Mam Tor in Derbyshire is shown in relation to both the suitability of ascending/descending modes with respect to local slope orientation, and land cover distribution for landslide deposits. Analogously, in Figs. 16 and 17 we summarize the visibility maps to the ERS-1/2 and ENVISAT modes and the calibrated CLC2006 map with predicted PS densities for two landslide areas in southern England, i.e. Folkestone Warren in Kent and Undercliff in the Isle of Wight.

The first area shows that the ascending geometry provides a better picture of local terrain and allows minimization of layover within the area of landslide deposits of Folkestone Warren, whilst the descending mode is generally not suitable to image the slope due to its predominantly south-east aspects and presence of layover dominating the landslide scarp (Fig. 16). The orientation of the descending LOS would also result in the underestimation of down slope motions, these being almost perpendicular to the LOS and thus not seen by conventional InSAR, PSI or SBAS methods. Low likelihood to retrieve PS is observed for the vast majority of the deposit, and higher potential for PSI methods is found only for the towns of Capel le Ferne and Folkestone, where predicted PS densities reach class 2. On the other hand, we observe that the descending mode is very suitable to sense the unstable slopes in Undercliff of the Isle of Wight, with only small areas of radar layover found to the east of the cliff, for south and south-east facing steep slopes (Fig. 17). Suitability for PSI-like analysis reveals patchy distribution of predicted target densities, with peaks for the town of Niton (class 2), and lowest potential for PS identification in the central and western sectors of the deposits.

Building upon our assessment for landslides mapped across the national territory, we have identified test sites in Great Britain, over which we are carrying out SAR-based ground motion studies with ERS-1/2 and ENVISAT data covering the past 20 years. These sites

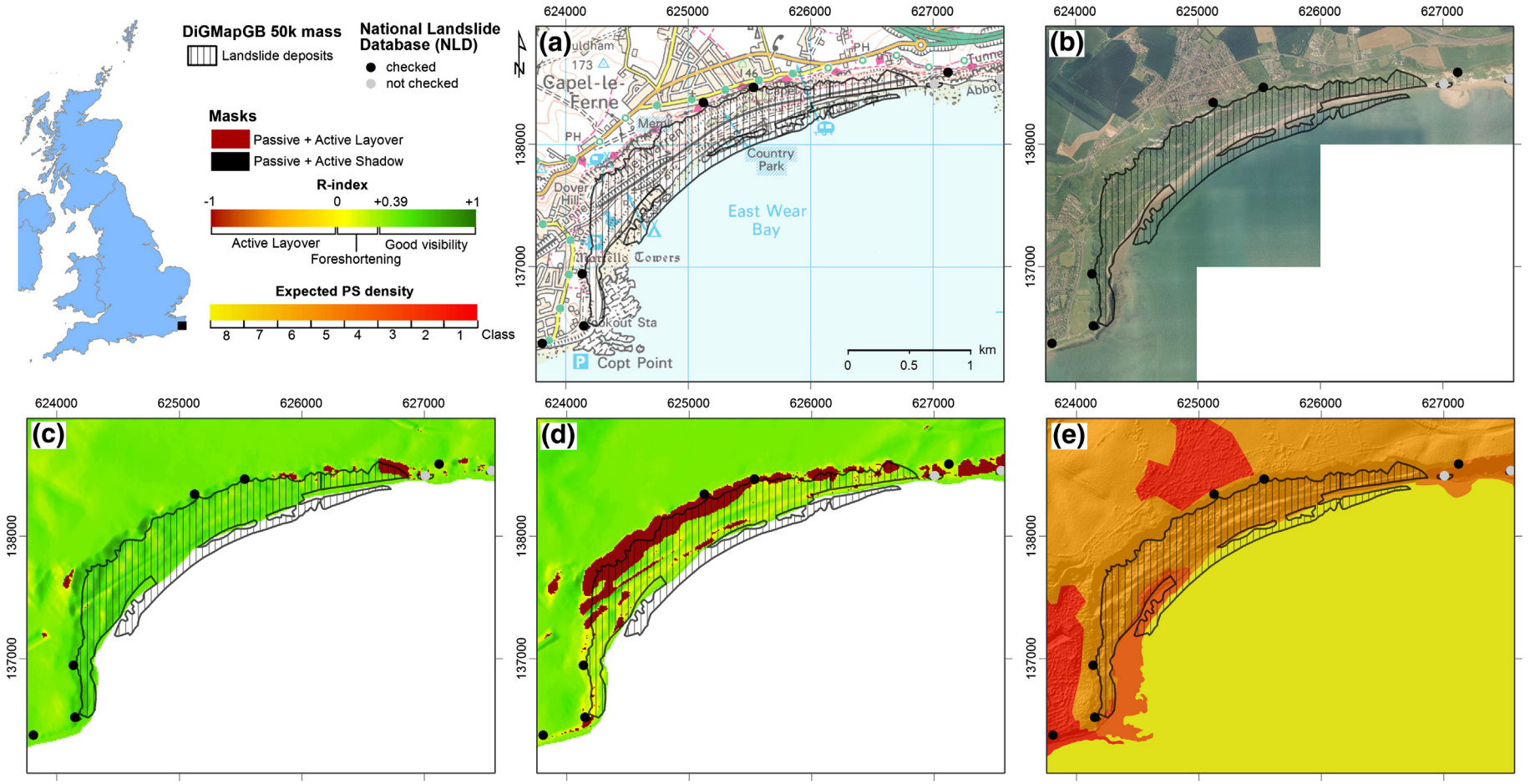

Fig. 16. DiGMapGB mass movement (landslide deposits) layer and NLD for the area of Folkestone Warren in southern England, overlapped onto: (a) OS 1:50,000 topographic base map, (b) 25 cm aerial photographs, (c–d) SAR topographic visibility maps to the ERS-1/2 and ENVISAT acquisition geometry in ascending (c) and descending (d) modes based on the 10 m NEXTMap® DTM, and (e) predicted PS densities from the calibrated CLC2006 map. OS data © Crown Copyright and database rights 2013. Aerial photography © UKP/Getmapping Licence No UKP2006/01. Geological materials © NERC, All rights reserved. NEXTMap® Britain © 2003, Intermap Technologies Inc., All rights reserved.

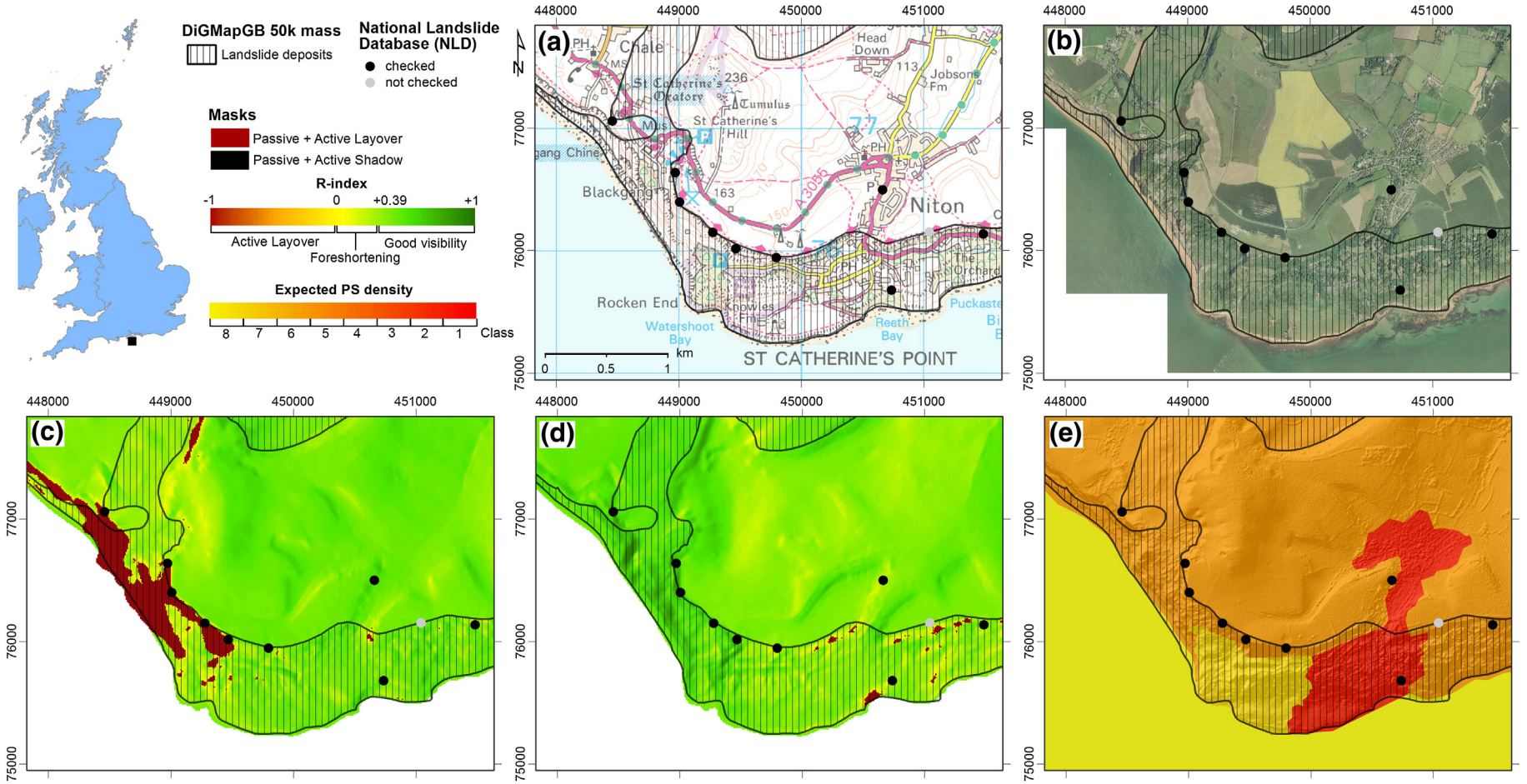

Fig. 17. DiGMapGB mass movement (landslide deposits) layer and NLD for the western sector of the Undercliff in the Isle of Wight, overlapped onto: (a) OS 1:50,000 topographic base map, (b) 25 cm aerial photographs, (c–d) SAR topographic visibility maps to the ERS-1/2 and ENVISAT acquisition geometry in ascending (c) and descending (d) modes based on the 10 m NEXTMap® DTM, and (e) predicted PS densities from the calibrated CLC2006 map. OS data © Crown Copyright and database rights 2013. Aerial photography © UKP/Getmapping Licence No UKP2006/01. Geological materials © NERC, All rights reserved. NEXTMap® Britain © 2003, Intermap Technologies Inc., All rights reserved.

include Wales and The Pennines, landslides affecting transport infrastructure in Folkestone Warren, Broken Bank and Rest-And-Be-Thankful, and coastal sites in the Isle of Wight and Cayton Bay.

5. Conclusions and future perspectives

The feasibility of SAR imaging data to study Britain has been analysed in relation to the availability of archived stacks of imagery suitable for (non-)interferometric applications, terrain visibility to the radar sensor modes, and the likelihood of the various land cover types to provide good radar reflectors to monitor with PSI methods.

We showed that topography exerts limited control on the visibility of the British landmass, with only ~1.0–1.4% of the total territory potentially affected by radar shadow and layover to the ERS-1/2 and ENVISAT modes in each acquisition mode according to the 50 m to 5 m resolution DTM-based simulations. Simulated layover and shadow regions were obtained by employing constant LOS incidence angle θ (23°) and ground track angle γ (14°) across the scene. Differences of the simulated layover areas with respect to those computed by considering θ variations across the swath were found to be as little as −7% and +8.5% at the near and far range (where θ is ~19° and ~27°). Validation in South Wales with ERS-2 data also confirmed that the approach performs well and showed that the difference between simulated and observed layover equalled ~10% of the total layover identified across the scene when using a DTM with resolution lower than that of the analysed SAR imagery. Thus the national area that could be potentially affected by distortions equals ~0.9–1.3% based on the DTM simulations, and the extension of distortions across the landmass can be still considered negligible. Areas resulting in layover or shadow distortions in both geometries, i.e. areas that cannot be monitored using SAR imagery with either orbital mode cover only 0.02–0.04% of the landmass. Our study of the effect of scale of the input DTM resolution on the discrimination of SAR distortions helped to understand how the various resolutions are capable to depict the terrain complexity and to identify the most suitable resolution to perform such a simulation. Although in our analysis with medium resolution imagery the NEXTMap® dataset at 10 m resolution could be considered as the ideal input DTM to perform the simulation, the errors observed using the 50 m resolution DTM proved that the simulation can still be considered reliable in case of the absence of more detailed terrain models. The latter represents a possible operational scenario, when only low or medium resolution topographic datasets are available for the target areas of interest, such as the SRTM DSM at 90 m or the ASTER Global DEM (GDEM) at 30 m, both freely available for the majority of the Earth's surface. In these cases, such elevation models can still be used to assess with sufficient accuracy the visibility of the target areas to the SAR sensor geometry prior to image acquisition and processing.

Calibration of the CLC2006 dataset using external PS data for London, Stoke-On-Trent, Newcastle and Bristol, allowed characterisation of the various land cover classes in terms of the potential PS density that they could provide over Britain. Despite the predominance of non-urban land cover across the landmass, we estimate that the potential number of PS targets that could be identified by processing a set of image frames covering Great Britain should exceed 12.8 M points for each acquisition mode. We validated the calibrated CLC2006 map with the observed distribution of IPTA ERS-1/2 candidates in South Wales. Relative PS density and rankings among the land cover classes were found constant across the different datasets, although absolute differences between observed and predicted densities appeared significant, and a ratio of 5 has been found between observed and predicted targets in South Wales. The total number of PS predicted for Great Britain was therefore rescaled to account for this factor, and thus obtaining potential for over 2.5 M targets across the landmass.

The above figure is clearly influenced by a series of factors relating to the input satellite data and their processing methods. Indeed, results obtained by other authors demonstrate that the number of identified radar targets increases if:

(i) the input data stacks have shorter repeat cycles and revisiting times.
Ferretti, Colesanti, Perissin, Prati, and Rocca (2003) studied the impact of temporal decorrelation and satellite repeat-cycles on the identification of PS, semi-PS and temporary-PS, by comparing results with 35-day and 3-day repeat cycle ERS data. The authors found that shorter revisiting times result in much higher PS densities than those with monthly acquisition frequencies, due to reduced temporal decorrelation, hence loss of coherence of the imaged targets in the latter case. This evidence clearly plays a key role for future C-band SAR missions with shorter repeat cycles, such as ESA's Sentinel-1 constellation with 12 day repeat cycles per satellite (Torres et al., 2012), which might enhance further the potential of C-band SAR stacks being succeeding the ERS and ENVISAT missions.

(ii) higher resolution SAR data are used.
Bianchini, Cigna, Del Ventisette, Moretti, and Casagli (2013) observe over 3200 TerraSAR-X SpotLight PS/km^2 over a mixed urban and rural land cover area in Italy analysed with the Persistent Scatterer Pairs (PSP-IFSAR) technique. Crosetto et al. (2010) highlight that the density of TerraSAR-X StripMap PS over urban areas can be as high as 47 times higher than that generated by processing an equivalent stack of ENVISAT IS2 ASAR data. Wasowski et al. (2014) retrieve over 1000 PS/km^2 when processing COSMO-SkyMed StripMap data by using the Stable Point INterferometry over Un-urbanised Areas (SPINUA) technique, and Bovenga, Wasowski, Nitti, Nutricato, and Chiaradia (2012) obtain 3 to 11 times higher densities of radar targets using COSMO-SkyMed StripMap compared to ENVISAT IS2 ASAR imagery. From these observations, it is evident that the use of higher resolution data would increase the total number of scatterers that could be identified over the entire territory of Britain. For instance, based on the results of our feasibility mapping and according to the evidence shown by Bovenga et al. (2012), the projected number of targets that may be identified over Great Britain by using COSMO-SkyMed StripMap data may exceed a total of 25 M scatterers per acquisition mode, which would represent an unprecedented and invaluable source of information on terrain motions affecting the landmass. These scatterers, however, would mostly be in urban areas.

(iii) improved processing techniques are employed.
Ferretti et al. (2011) show that the spatial density of RADARSAT-1 Measurement Points (MP) in the Italian Alps increases from 85 to 450 MP/km^2 when comparing the results of a conventional PSInSAR™ processing with those from SqueeSAR™. Tapete, Fanti, Cecchi, Petrangeli, and Casagli (2012) also study semi-urban, rural, archaeological areas in Rome (Italy), and report on target densities as high as ~1200–3000 MP/km^2 with datasets processed with SqueeSAR™. Although being conceptually different from PSI-like approaches, the Intermittent SBAS (ISBAS; Sowter et al., 2013) has also proved able to identify more targets over a wide range of land cover classes, including agriculture and grassland and other land covers with lower likelihoods of resulting in good target densities. ISBAS applications in the Swadlincote and Coalville area in England (Sowter et al., 2013) and in the South Wales Coalfield (Bateson et al., in press) have shown greatly enhanced spatial coverage of ERS-1/2 and ENVISAT monitoring results with respect to standard SBAS methods.

For Britain, the success of any SAR-based analysis of unstable slopes and landslide deposits as mapped in the DiGMapGB and NLD for hilly and mountainous regions of Great Britain is controlled by the sensor acquisition geometry and the presence of image distortions, though the

mutual use of ascending and descending modes compensates for the issues related to SAR distortions for most landslide affected areas. The results of our feasibility assessment show significant control of land cover on the potential for PS methods to identify scatterers, with particularly critical evidence for rural and grassland regions where only a few radar targets per square kilometre can be extracted and monitored via multi-interferogram processing (see Section 2.3). This suggests that higher image resolutions and shorter repeat-cycles would only partially address the need for more dense networks of monitoring targets across rural and partly-vegetated regions.

Newly developed techniques such as SqueeSAR™ and ISBAS have demonstrated that remarkable improvements in the number and density of identified targets in non-urban areas can be achieved by working on distributed scatterers (e.g., debris, non-cultivated land, or low vegetation cover) in case of SqueeSAR™, or intermittently coherent surfaces in the case of ISBAS, and therefore seem capable of addressing this need for Britain. It seems apparent that these new processing methods may provide a solution to the problem of lack or extremely low density of targets that can be identified and monitored by employing the existing C-band archives of ERS-1/2 and ENVISAT satellites with other processing techniques. Indeed, C-band SAR coherence over rural areas of Britain is generally very low (e.g., Bateson et al., in press) and likely to result in insufficiently dense networks of monitoring targets, with little possibility to obtain full understanding of terrain motions. For these reasons, improved techniques and methods which are capable to further exploit the potential of C-band archives over rural and semi-vegetated areas appear indispensable to enhance InSAR-based landslide research and monitoring in Great Britain.

Acknowledgements

This research was funded by the British Geological Survey (BGS), Natural Environment Research Council (NERC) via the OF55 FY12-13 research project “Assessing the feasibility of EO technologies (InSAR) for nationwide monitoring of geohazards in GB: first applications to landslide hazards” led by F. Cigna, C. Jordan and C. Dashwood. ERS-1/2 SAR data were provided by ESA via the Category-1 project id.13543 “Enhancing landslide research and monitoring capability in Great Britain using C-band satellite SAR imagery and change detection, InSAR and Persistent Scatterers techniques” led by F. Cigna (PI), and used for validation of the InSAR feasibility maps. Recomputed orbit solutions for ERS-1/2 data were made available by the Astrodynamics and Space Missions and the ESA/REAPER project, whilst PS datasets for London, Stoke-on-Trent, Bristol/Bath and Newcastle were made available through the projects ESA Terrafirma and EC-FP7 PanGeo. CORINE Land Cover 2006 data was made available by the European Environment Agency. NEXTMap® Britain elevation data was produced by Intermap Technologies, and pre-processed by Keith Adlam at BGS to generate derived 10 m and 50 m resolution DTMs for Britain. The feasibility assessment methodology was designed by F. Cigna and implemented with L. Bateson. ERS data processing was carried out by F. Cigna using the GAMMA SAR and Interferometry Software, developed by GAMMA Remote Sensing and Consulting AG (Switzerland) and licensed to BGS, NERC. This paper is published with permission of the Executive Director of BGS, NERC.

References

Adam, N., Rodriguez Gonzalez, F., Parizzi, A., & Liebhart, W. (2011). Wide area persistent scatterer interferometry. *2011 IEEE International Geoscience and Remote Sensing Symposium (IGARSS 2011)* (pp. 1481–1484) (Vancouver, BC).

Aldiss, D., Burke, H., Chacksfield, B., Bingley, R., Teferle, N., Williams, S., et al. (2014). Geological interpretation of current subsidence and uplift in the London area, UK, as shown by high precision satellite-based surveying. *Proceedings of the Geologists Association*, *125*, 1–13.

Bally, P. (Ed.). (2012). *Scientific and Technical Memorandum of The International Forum on Satellite EO and Geohazards, 21–23 May 2012, Santorini, Greece*. ESA/ESRIN.

Banton, C., Bateson, L., Mccormack, H., Holley, R., Watson, I., Burren, R., et al. (2013). Monitoring post-closure large scale surface deformation in mining areas. *Mine Closure 2013, Eighth International Conference on Mine Closure*. Eden Project, Cornwall, UK: Australian Centre for Geomechanics, Perth.

Barboux, C., Delaloye, R., Strozzi, T., Collet, C., & Raetzo, H. (2011). TSX assessment for slope instabilities monitoring in Alpine periglacial environment (Western Swiss Alps, Switzerland). *Fringe 2011 Workshop, 19–23 September 2011*. Frascati, Italy: ESA/ESRIN.

Bateson, L., Cigna, F., Boon, D., & Sowter, A. (2014). The application of the Intermittent SBAS (ISBAS) InSAR method to the South Wales Coalfield, UK. *International Journal of Applied Earth Observation and Geoinformation* (in press).

Berardino, P., Fornaro, G., Lanari, R., & Sansosti, E. (2002). A new algorithm for surface deformation monitoring based on small baseline differential SAR interferograms. *IEEE Transactions on Geoscience and Remote Sensing*, *40*, 2375–2383.

Bianchini, S., Cigna, F., Del Ventisette, C., Moretti, S., & Casagli, N. (2013). Monitoring landslide-induced displacements with TerraSAR-X Persistent Scatterer Interferometry (PSI): Gimigliano case study in Calabria Region (Italy). *International Journal of Geosciences*, *4*(10), 1467–1482. http://dx.doi.org/10.4236/ijg.2013.410144.

Bovenga, F., Wasowski, J., Nitti, D. O., Nutricato, R., & Chiaradia, M. T. (2012). Using COSMO/SkyMed X-band and ENVISAT C-band SAR interferometry for landslides analysis. *Remote Sensing of Environment*, *119*, 272–285.

Caro Cuenca, M., Hanssen, R., Hooper, A., & Arıkan, M. (2011). Surface deformation of the whole Netherlands after PSI analysis. *FRINGE 2011 Workshop, ESA SP-697* (pp. 1–8). Frascati, Italy: ESA/ESRIN.

Cascini, L., Fornaro, G., & Peduto, D. (2010). Advanced low- and full-resolution DInSAR map generation for slow-moving landslide analysis at different scales. *Engineering Geology*, *112*, 29–42.

Cigna, F., Bateson, L., Jordan, C., & Dashwood, C. (2012). Feasibility of InSAR technologies for nationwide monitoring of geohazards in Great Britain. *Remote Sensing and Photogrammetry Society (RSPSoc) — Annual Conference 2012* (pp. 1–4). London, UK: RSPSoc.

Cigna, F., Bateson, L., Jordan, C., & Dashwood, C. (2013). Nationwide monitoring of geohazards in Great Britain with InSAR: Feasibility mapping based on ERS-1/2 and ENVISAT imagery. *2013 IEEE International Geoscience and Remote Sensing Symposium (IGARSS 2013)* (pp. 672–675). http://dx.doi.org/10.1109/IGARSS.2013.6721246.

Cigna, F., Bianchini, S., & Casagli, N. (2013). How to assess landslide activity and intensity with Persistent Scatterer Interferometry (PSI): The PSI-based matrix approach. *Landslides*, *10*, 267–283.

Colesanti, C., & Wasowski, J. (2006). Investigating landslides with space-borne Synthetic Aperture Radar (SAR) interferometry. *Engineering Geology*, *88*, 173–199.

Colombo, A., Mallen, L., Pispico, R., Giannico, C., Bianchi, M., & Savio, G. (2006). Mappatura regionale delle aree monitorabili mediante l'uso della tecnica PS. *10th National Conference ASITA, 14–17 November 2006* (Bolzano, Italy).

Costabile, S. (2012). Persistent Scatterer Interferometry and Cosmo-SkyMed data in the Piano Straordinario di Telerilevamento Ambientale (PST-A). In E-GEOS (Ed.), *E-GEOS Conference 2012* (Rome, Italy).

Crosetto, M., Monserrat, O., Iglesias, R., & Crippa, B. (2010). Persistent scatterer interferometry: Potential, limits and initial C- and X-band comparison. *Photogrammetric Engineering and Remote Sensing*, *76*, 1061–1069.

Culshaw, M., Tragheim, D., Bateson, L., & Donnelly, L. (2006). Measurement of ground movements in Stoke-on-Trent (UK) using radar interferometry. In Culshaw et al. (Eds.), *IAEG 2006, Engineering geology for tomorrow's cities, 10th Congress of the International Association for Engineering Geology and the Environment* (pp. 1–10). Nottingham, UK: Geological Society, London.

EC (2011). *Mapping guide for a European Urban Atlas*. European Commission (EC), 1–31 (Available at: http://www.eea.europa.eu/data-and-maps/data/urban-atlas/. Accessed on: 11/03/2014).

EEA (2007). CLC2006 technical guidelines. *European Environment Agency (EEA) Technical report No.17/2007* (pp. 70) (Available at: http://www.eea.europa.eu/publications/technical_report_2007_17. Accessed on: 11/03/2014).

EEA (2012). *Implementation and achievements of CLC2006*. 65 (Available at: http://www.eea.europa.eu/data-and-maps/data/corine-land-cover-2006-raster-2/clc-final-report/clc-final-report. Accessed on: 11/03/2014).

ESA (2007). *Envisat ASAR product handbook*. Issue 2.2 — European Space Agency (ESA), 564 (Available at: https://earth.esa.int/pub/ESA_DOC/ENVISAT/ASAR/asar.ProductHandbook.2_2.pdf. Accessed on: 11/03/2014).

ESA (2009). *The Terrafirma Atlas. Terrain-motion across Europe*. A compendium of results produced by the European space agency GMES service element project Terrafirma 2003–2009, 94 (Available at: http://esamultimedia.esa.int/multimedia/publications/TerrafirmaAtlas/pageflip.html. Accessed on: 11/03/2014).

ESA (2014a). First Copernicus satellite at launch site. Available at: http://www.esa.int/Our_Activities/Observing_the_Earth/Copernicus/First_Copernicus_satellite_at_launch_site (Accessed on: 11/03/2014)

ESA (2014b). Sentinel-1. Available at: http://www.esa.int/Our_Activities/Observing_the_Earth/Copernicus/Sentinel-1 (Accessed on: 11/03/2014)

Farrant, A.R., & Cooper, A. H. (2008). Karst geohazards in the UK: The use of digital data for hazard management. *Quarterly Journal of Engineering Geology and Hydrogeology*, *41*, 339–356.

Ferretti, A., Colesanti, C., Perissin, D., Prati, C., & Rocca, F. (2003). Evaluating the effect of the observation time on the distribution of SAR Permanent Scatterers. *FRINGE 2003, 1–5 December 2003*. Frascati, Italy: ESA/ESRIN.

Ferretti, A., Fumagalli, A., Novali, F., Prati, C., Rocca, F., & Rucci, A. (2011). A new algorithm for processing interferometric data-stacks: SqueeSAR. *IEEE Transactions on Geoscience and Remote Sensing*, *49*, 3460–3470.

Ferretti, A., Prati, C., & Rocca, F. (2001). Permanent scatterers in SAR interferometry. *IEEE Transactions on Geoscience and Remote Sensing*, *39*, 8–20.

Foster, C., Pennington, C. V. L., Culshaw, M. G., & Lawrie, K. (2012). The national landslide database of Great Britain: Development, evolution and applications. *Environmental Earth Sciences*, *66*, 941–953.

Gelautz, M., Frick, H., Raggam, J., Burgstaller, J., & Leberl, F. (1998). SAR image simulation and analysis of alpine terrain. *ISPRS Journal of Photogrammetry and Remote Sensing*, *53*, 17–38.

Gibson, A.D., Culshaw, M. G., Dashwood, C., & Pennington, C. V. L. (2013). Landslide management in the UK—The problem of managing hazards in a 'low-risk' environment. *Landslides*, *10*, 599–610.

Herrera, G., Gutiérrez, F., García-Davalillo, J. C., Guerrero, J., Notti, D., Galve, J. P., et al. (2013). Multi-sensor advanced DInSAR monitoring of very slow landslides: The Tena Valley case study (Central Spanish Pyrenees). *Remote Sensing of Environment*, *128*, 31–43.

Hulme, M., Jenkins, G. J., Lu, X., Turnpenny, J. R., Mitchell, T. D., Jones, R. G., et al. (2002). *Climate change scenarios for the United Kingdom: The UKCIP02 scientific report.* Norwich, UK: Tyndall Centre, School of Environmental Sciences, University of East Anglia (118 pp.).

Jones, L. D., & Jefferson, I. (2012). Expansive soils. In J. Burland (Ed.), *ICE manual of geotechnical engineering. Geotechnical engineering principles, problematic soils and site investigation, Vol. 1.* (pp. 413–441). London, UK: ICE Publishing.

Kropatsch, W. G., & Strobl, D. (1990). The generation of SAR layover and shadow maps from digital elevation models. *IEEE Transactions on Geoscience and Remote Sensing*, *28*, 98–107.

Leighton, J. M., Sowter, A., Tragheim, D., Bingley, R. M., & Teferle, F. N. (2013). Land motion in the urban area of Nottingham observed by ENVISAT-1. *International Journal of Remote Sensing*, *34*, 982–1003.

Met Office (2013a). *Fact sheet No. 4 — Climate of the British Isles.* National Meteorological Library and Archive (Available at: http://www.metoffice.gov.uk/learning/library/publications/factsheets. Accessed on: 11/03/2014).

Met Office (2013b). UK climate and weather statistics. UK climate averages for 1981–2010: Summary of key features. Available at: http://www.metoffice.gov.uk/weather/uk/climate.html (Accessed on: 11/03/2014)

Morton, D., Rowland, C., Wood, C., Meek, L., Marston, C., Smith, G., et al. (2011). Final report for LCM2007 — The new UK Land Cover Map. Available at: *Countryside Survey Technical Report No.11/07 NERC/Centre for Ecology & Hydrology* (pp. 112) (Available at: http://www.countrysidesurvey.org.uk/sites/default/files/pdfs/LCM2007%20Final%20Report%20-%20vCS%20Web.pdf. Accessed on: 11/03/2014).

Nico, G., Oliveira, S., Catalão, J., & Zêzere, J. L. (2009). On the statistical properties of persistent scatterers location to discriminate landslide predisposing factors. *Fringe 2009 Workshop*. Frascati, Italy: ESA.

Notti, D., Davalillo, J. C., Herrera, G., & Mora, O. (2010). Assessment of the performance of X-band satellite radar data for landslide mapping and monitoring: Upper Tena Valley case study. *Natural Hazards and Earth System Sciences*, *10*, 1865–1875.

Notti, D., Meisina, C., Zucca, F., & Colombo, A. (2011). Models to predict Persistent Scatterers data distribution and their capacity to register movement along the slope. *Fringe 2011 Workshop, 19–23 September 2011*. Frascati, Italy: ESA/ESRIN.

Plank, S., Singer, J., Minet, C., & Thuro, K. (2010). GIS based suitability evaluation of the differential radar interferometry method (D-InSAR) for detection and deformation monitoring of landslides. *FRINGE 2009, 30 Nov.–4 Dec. 2009* (pp. 1–8). Frascati, Italy: ESA.

Plank, S., Singer, J., Minet, C., & Thuro, K. (2012). Pre-survey suitability evaluation of the differential synthetic aperture radar interferometry method for landslide monitoring. *International Journal of Remote Sensing*, *33*, 6623–6637.

Plank, S., Singer, J., & Thuro, K. (2013). Assessment of number and distribution of persistent scatterers prior to radar acquisition using open access land cover and topographical data. *ISPRS Journal of Photogrammetry and Remote Sensing*, *85*, 132–147.

Pourthie, N., Sand, A., Fjortoft, R., Koudogbo, F., Duro, J., Urdiroz, A., et al. (2010, 31 May–3 Junee). SARVisor: An integrated tool to facilitate SAR data selection. *30th EARSeL Symposium Remote Sensing for Science, Education, and Natural and Cultural Heritage* (pp. 45–52). Paris, France: UNESCO.

Riddick, S. N., Schmidt, D. A., & Deligne, N. I. (2012). An analysis of terrain properties and the location of surface scatterers from persistent scatterer interferometry. *ISPRS Journal of Photogrammetry and Remote Sensing*, *73*, 50–57.

Rodriguez Gonzalez, F., Adam, N., Parizzi, A., & Brcic, R. (2013). The integrated wide area processor (IWAP): A processor for wide area persistent scatterer interferometry. *ESA Living Planet Symposium 2013*. Edinburgh, UK: ESA/ESRIN.

Rosen, P. A., Hensley, S., Joughin, I. R., Fuk, K. L., Madsen, S. N., Rodriguez, E., et al. (2000). Synthetic aperture radar interferometry. *Proceedings of the IEEE*, *88*, 33–382.

Smith, A. (2013a). *Digital Geological Map of Great Britain, information notes, 2013.* British Geological Survey Open Report, 54 (Nottingham, UK, Available at: http://nora.nerc.ac.uk/502315/. Accessed on: 11/03/2014).

Smith, A. (2013b). *User guide for the BGS DiGMapGB-50 data (V7)*. British Geological Survey Open Report, 11 (Nottingham, UK, Available at: http://nora.nerc.ac.uk/502313/. Accessed on: 11/03/2014).

Sowter, A., Bateson, L., Strange, P., Ambrose, K., & Syafiudin, M. (2013). DInSAR estimation of land motion using intermittent coherence with application to the South Derbyshire and Leicestershire coalfield. *Remote Sensing Letters*, *4*, 979–987.

Strozzi, T., Ambrosi, C., & Raetzo, H. (2013). Interpretation of aerial photographs and satellite SAR interferometry for the inventory of landslides. *Remote Sensing*, *5*, 2554–2570.

Tapete, D., & Cigna, F. (2012). Rapid mapping and deformation analysis over cultural heritage and rural sites based on Persistent Scatterer Interferometry. *International Journal of Geophysics*, 618601–618619 (ID 618609).

Tapete, D., Fanti, R., Cecchi, R., Petrangeli, P., & Casagli, N. (2012). Satellite radar interferometry for monitoring and early-stage warning of structural instability in archaeological sites. *Journal of Geophysics and Engineering*, *9*, S10.

Torres, R., Snoeij, P., Geudtner, D., Bibby, D., Davidson, M., Attema, E., et al. (2012). GMES Sentinel-1 mission. *Remote Sensing of Environment*, *120*, 9–24.

Wasowski, J., Bovenga, F., Dijkstra, T., Meng, X., Nutricato, R., & Chiaradia, M. (2014). Persistent Scatterers Interferometry provides insight on slope deformations and landslide activity in the mountains of Zhouqu, Gansu, China. In K. Sassa, P. Canuti, & Y. Yin (Eds.), *Landslide science for a safer geoenvironment* (pp. 359–364). Springer International Publishing.

Werner, C., Wegmuller, U., Strozzi, T., & Wiesmann, A. (2003). Interferometric point target analysis for deformation mapping. *2003 IEEE International Geoscience and Remote Sensing Symposium (IGARSS 2003)* (pp. 4362–4364).